Journal of African Earth Sciences
January 2023, Volume 197, Pages 104765 (13p.)
https://doi.org/10.1016/j.jafrearsci.2022.104765
https://archimer.ifremer.fr/doc/00799/91132/

Archimer
https://archimer.ifremer.fr

Mixed carbonate-siliceous hydrothermal chimneys ahead of the Asal propagating rift (SE Afar Rift, Republic of Djibouti)

Moussa Nima [1, *], Bayon Germain [2], Dekov V. [3], Yamanaka T. [3], Shinjo R. [4, 5], Toki T. [5, 6], Le Gall Bernard [7], Grassineau N. [8], Langlade Jessica [9], Awaleh M.O. [1], Pelleter Ewan [2]

[1] Institut des Sciences de la Terre, Centre d'Etudes et de Recherches de Djibouti, B.P. 486, Djibouti
[2] Univ Brest, CNRS, Ifremer, Geo-Ocean, F-29280, Plouzané, France
[3] Department of Ocean Sciences, Tokyo University of Marine Science and Technology, 4-5-7 Konan, Minato-ku, Tokyo, 108-8477, Japan
[4] Department of Physics and Earth Sciences, Faculty of Science, University of the Ryukyus, 1 Senbaru, Nishihara, Okinawa, 903-0213, Japan
[5] Research Institute for Humanity and Nature, 457-4 Motoyama, Kamigamo, Kita-ku, Kyoto, 603-8047, Japan
[6] Department of Chemistry, Biology and Marine Science, Faculty of Science, University of the Ryukyus, 1 Senbaru, Nishihara, Okinawa, 903-0213, Japan
[7] UMR/CNRS 6538 Géosciences Océan, UBO-IUEM, Place Nicolas Copernic, 29280, Plouzané, France
[8] Department of Earth Sciences, Royal Holloway University of London, EGHAM Surrey, TW20 0EX, UK
[9] CNRS, IUEM, UMS 3113, F-29280, Plouzané, France

* Corresponding author : Nima Moussa, email address : nmoussae@gmail.com

Abstract :

Numerous active and fossil hydrothermal carbonate chimneys have been reported at Lake Asal and Lake Abhe, in the southeastern part of the Afar Rift (Republic of Djibouti): a tectonically and volcanically active region for the last 30 million years. In this study, we report on a detailed mineralogical and geochemical investigation of unusual hydrothermal mixed carbonate-siliceous chimneys recently discovered in the Allols area (Harralol, Haralé Awda and Sakallol), northwest of the Asal Rift. These inactive chimneys, up to 20 m high, consist of tall spires partly stained by Fe-oxides. They are located along major faults and were formed sub-aqueously when the area was occupied by a lake. Hydrothermal carbonate structures were also found in the same area. The oxygen (δ18O) and carbon (δ13C) isotopic compositions of the chimneys range from −4.5 to 25.3‰ and from −9.44 to 8.92‰, respectively, indicating mixing between magmatic and surficial waters. Their radiogenic Sr isotopic compositions ($^{87}Sr/^{86}Sr = 0.7049–0.7056$) show values typical of altered basaltic rocks. Chimneys also exhibit negative Ce anomaly suggestive of a genetic link with basalt alteration. Overall, this study suggests that lake water chemistry in the Allols area experienced major changes in the past, reflecting various contributions of mixing fluids (lake water and hydrothermal fluids), leading alternatively to deposition of carbonate chimneys and precipitation of (and/or replacement with) silica.

Please note that this is an author-produced PDF of an article accepted for publication following peer review. The definitive publisher-authenticated version is available on the publisher Web site.

Graphical abstract

Schematic model of the studied area, which shows the relation between the Sakallol basins hydrothermal precipitation, groundwater and seawater from the Ghoubbet al-Kharab (Not at scale).

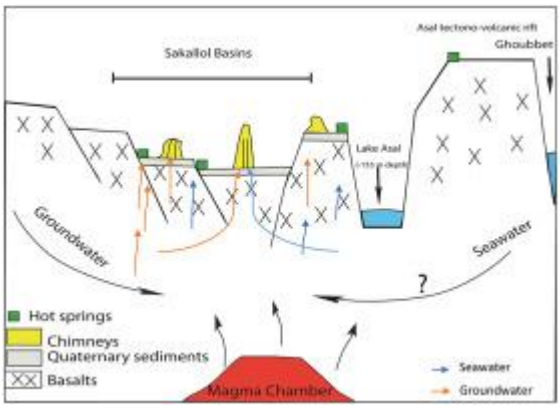

Highlights

► Hydrothermal chimneys ahead of the Asal propagating rift, SE Afar Rift, Republic of Djibouti. ► Radiogenic Sr isotopic compositions ($^{87}Sr/^{86}Sr$) range from 0.7049 to 0.7056 ► $\delta^{18}O$ and $\delta^{13}C$ values of the chimneys range from −4.5 to 25.3‰ and from −9.44 to 8.92‰. ► Negative Ce anomaly indicate basaltic alteration. ► Mixing fluids such as lake water and hydrothermal fluids which allowed the deposition of carbonate chimneys and precipitation of (and/or replacement with) silica.

Keywords : SE Afar Rift, hydrothermal chimneys, isotopic analyses, Allols sites, Djibouti

Please note that this is an author-produced PDF of an article accepted for publication following peer review. The definitive publisher-authenticated version is available on the publisher Web site.

1. Introduction

Since the end of the 1970s, more than 500 hydrothermal fields have been discovered and studied in various seafloor settings such as mid-ocean ridges, back-arc basins, volcanic arcs, hot spots, or continental rifts (Rona, 1984; Fouquet et al., 2010). Despite extensive research conducted on modern hydrothermal deposits, focused mainly on sulfide and sulfate mineralizations, limited work has been done on silica-rich hydrothermal chimneys (Herzig et al., 1988; Juniper and Fouquet, 1988; Shanks et al., 2005; Dekov et al., 2015).

The southeastern part of the Afar Rift (Republic of Djibouti) is the location of extensive tectonics, volcanic and hydrothermal activity (Fig. 1A) (Stieljes, 1973; De Chabalier and Avouac, 1994; Deniel et al., 1994; Pinzutti et al., 2013). Over the last decades, the discovery of many hot springs and fumaroles in this region has fostered major interest in geothermal exploration (Fontes et al., 1989; San Juan et al., 1990; D'Amore et al., 1998; Awaleh et al., 2015a, b; 2017). Since the 1970s, many hydrothermal structures have also been identified in the lakes that are aligned along the rift system (e.g. Lake Asal and Lake Abhé; Fig. 1A). Most of these hydrothermal edifices correspond to carbonate chimneys, formed in alkaline-to-mildly acidic lake waters (Gasse and Fontes, 1989; Dekov et al., 2014; 2021).

In this contribution, we report the results of field and geochemical investigations of unusual hydrothermal deposits discovered in a dessicated saline lake located in the Allols depression, in the NW prolongation of the Asal rift axis (Fig. 1). These precipitates were formed as a result of sub-lacustrine hydrothermal activity, corresponding to the occurrence of up to 20-m-tall inactive tower-like silica-rich chimneys, associated with stromatolite-like carbonate deposits (Fig. 1B). Both carbonate and silica-rich towers are also present in a veneer crowning the surrounding basaltic escarpment, suggesting that the chimneys were

formed during a period of high lake level (Fig. 1C, D). The Sakallol chimneys resemble in form and size the hydrothermal carbonate chimneys found at nearby Lake Abhé and Lake Asal (Gasse and Fontes, 1989; Dekov et al., 2014; 2021), but unlike these latter chimneys, some of the Sakallol chimneys are highly enriched in silica.

In this work, we report on the mineralogical and geochemical composition (including C-O-Sr-U-Th isotopes) of these peculiar chimney-like structures from the Sakallol depression with the aim to understand their origin and to propose a genetic model in relation with the regional tectono-volcanic evolution and lake water level fluctuations.

2. Geological setting

The Afar Rift in Djibouti area includes various rock formations that range chronologically as follows: the Ali Sabieh intrusive/effusive mafic series (28-21 Ma); the widespread Mablas rhyolites (15-11 Ma); the Dalha basalts (9-4 Ma); the Stratoid-Gulf basaltic series (3-1 Ma), which covers most of the Afar depression; and finally the youngest and more localized Asal volcanics (Stieljes, 1973; Gasse et al., 1986; Le Gall et al., 2010). The axial and active zones of the SE Afar rift currently occur along the Asal rift and its NE extent in the Manda-Inakir range (Manighetti et al., 1998) (Fig. 1A). This exposed rift system represents the emerged tip zone of the westerly-propagating Gulf of Aden-Tadjoura spreading ridge, *via* a marked clockwise deviation in the Ghoubbet/Tadjoura transition zone (Fig. 1) (Stieljes, 1973; Barberi and Varet, 1977; Manighetti et al., 1998; Audin et al., 2001; Daoud et al., 2011). Lake Asal occupies an exceptional geological, topographical and hydrogeological setting along the tectonically active floor of the Asal Rift (Fig. 1). It is located at 155 m below

sea level, separated from the Ghoubbet sea arm to the SE by the Fieale central volcano, which has thus acted as a plug since the last 300 kyr (Gasse and Fontes, 1989). Lake Asal is one of the few modern examples worldwide of a marine-fed rift basin that actively accumulates evaporite deposits, being located in the youngest and deepest basin of a suite of enclosed depressions down faulted through a thick sequence of stratified basalts, which includes, from West to East: the river-fed lake Abhé basin, the Hanlé-Dobi, the Gagaddé, and the Asal-Harralol-Sakallol depressions (Fig. 1; Gasse and Fonte, 1989).

The Manda-Inakir Range, at the boundary between the Danakil Horst and the Afar Depression, has been the locus of extensional tectonics between 4 and 1 Ma (Vellutini, 1990). This range is composed of two rifting zones (Fig. 1B). The Manda range is mainly located in Ethiopia and only its southern part extends in Djibouti with a NW-SE direction (Vellutini, 1990; Manighetti et al., 1998). The second rift is the Inakir structure located near Dorra (Fig. 1A). It is a NW-SE upwarping of the Stratoid series with a 2-3 km wide axis. Many basaltic cinder cones, built on the bordering faults of the rift-emitted lavas flows on the external slope of the upwelling (Vellutini, 1990).

The Harralol-Haralé Awda and Sakallol areas are located in the northwest region of the Asal Rift. The physiography of the basins is dominated by NW-SE fault scarps, which exceed 500 m in height. The lowest elevation of these basins is slightly below sea level. Between 8600 and 6000 yr before present (BP), the Lake Asal and Allol depressions (Harralol-Haralé Awda, Sakallol) were connected by channels (Gasse and Fontes, 1989). At that time, the Sakallol depression was occupied by a lake reaching at least 40 m in depth (Gasse, 1975).

In this area, bedrock is composed of 3-to-1 Ma old Stratoid basalts. The Harralol-Haralé Awda and Sakallol basins are infilled with diatom-rich Quaternary sediments and various hydrothermal structures (Fig. 2**)**. The Harralol depression is characterized by alluvial and salt

deposits. The Dalha basalts outcrop along the eastern edge of the depression. The hot spring waters in these basins display high concentrations of sodium bicarbonate and sodium chloride (Awaleh et al., 2017). Travertine and stromatolite-like structures, and other carbonate deposits are distributed along major faults (Fig. 1D). These deposits are locally covered by subaquatic or subaerial basaltic flows, hence reflecting the persistence of volcanic activity during and after corresponding lacustrine high stands.

The carbonate buildups at Sakallol are several meters high, located in the vicinity of active thermal springs and/or in veneer crowning the basaltic escarpment. Gasse and Fontes, (1989) reported that their formation began during the Lake Asal high stand, from ca. 6800 yr B.P.

3. Methodology

3.1. Mineralogical and geochemical analyses of bulk samples

Two types of chimney samples and surface sediments were collected for this study: chimneys located on the side of basaltic outcrops, and chimneys lying at the bottom of the Sakallol basin (Fig. 1 C; Fig. 2 A- B). A total of fifteen bulk samples were analyzed. Thin polished sections from carbonate and silica-rich chimneys were investigated by optical microscopy (Olympus BX50 polarizing microscope) and electron microprobe (Cameca SX100) at the “Microsonde Ouest” (IFREMER) for mineral composition and texture. The mineralogical composition of bulk samples was determined by X-Ray diffractometry (XRD; Brucker D8) with monochromatic CuKα radiation and scan from 5 to 70°2θ with step of 0.02°

at 5 s/step. In addition, X-ray elemental mapping was performed using a CAMECA SX100 electron microprobe with PAP correction program (Pouchou and Pichoir, 1984), under operating conditions of 15 kV accelerating voltage, 20 nA beam current and 1 μm^2 beam size.

The chemistry of bulk samples was analyzed for major and trace elements (SiO_2, Al_2O_3, Fe_2O_3, MgO, CaO, Na_2O, K_2O, TiO_2, P_2O_5, MnO, Ba, Co, Cu, Ni, Sc, Sr, V, Zn) by a Perkin Elmer Optima ICP-OES at the Earth Sciences Laboratory of Royal Holloway University of London (UK). A total of five geological CRMs (and two in-house RMs) were analysed during the analytical session: NIM-L (lujavrite), BE-N (basalt), DWA-1 (dolomite), CCH-1 (limestone) and GBW 07405 (soil). Samples were powdered, digested by fusion using lithium metaborate, and subsequently dissolved in 5% HNO_3 before ICP-OES analysis. For trace element analyses, the same samples were also separately digested with a mixture of concentrated HF-$HClO_4$-HCl, in accordance with the ISO 14869-1:2001 technique. The analytical precision was <10 % (RSD) for major element concentrations with >0.01 wt% and trace element abundances with >0.5 ppm. The accuracy was <10 % for major and trace element concentrations above 0.1 wt% and 0.5 ppm, respectively.

3.2. Trace element analyses of acid leachates

Additionally, a series of 17 samples collected along crosscut sections of 5 carbonate chimneys was leached with the aim to characterize trace element distribution in the carbonate-rich fraction (supposed to be authigenic) of studied chimneys, hence excluding any detrital component associated with terrigenous material. The leaching procedure included dissolution of bulk powdered samples (~20 mg) in diluted 2% (v/v) ultrapure HNO_3. The rare earth (REE) and other trace element (e.g. Zr, Hf, Sr, Y) abundances in the leachates were

171 determined using a Thermo Scientific Element XR sector field ICP-MS operated in low mass
172 resolution at the Pôle Spectrométrie Océan (PSO, Brest, France). Elemental concentrations
173 were calculated using the Tm addition method (Barrat et al., 1996). Isobaric interferences on
174 measured REE signals were corrected using oxide formation rates determined by analyzing
175 mono-elemental solutions of Ba-Ce, Nd-Pr, and Sm-Eu-Gd-Tb. In-run uncertainties on
176 measurements were generally better than 4% for all elements, and invariably <10%. The
177 analysis of in-house carbonate standard (BE-AN) yielded REE abundances in general
178 agreement (<13%) with recommended values of Barrat et al. (2020), except for Gd (>16%).
179 REE abundances are reported using the Post-Archean Australian shale (PAAS) reference
180 values (Pourmand et al., 2012).
181
182 *3.3. Isotopic composition*
183
184 *3.3.1. Carbon and oxygen isotopes*
185 For C and O isotopic analyses, bulk drilled and powdered samples from the
186 hydrothermal chimneys were analyzed by Isocarb prep-system using He Continuous-Flow
187 IRMS (Isoprime 100 Mass Spectrometer). The samples (~ 500 µg) were loaded into septum
188 screwed glass tubes flushed via auto sampler with He and evacuated in order to remove
189 atmospheric gases. Then, the samples were reacted with 500 µL 100% H_3PO_4 at 72°C for 1 h
190 in order to release CO_2 from carbonates following the standard methodology described by
191 McCrea (1950). Isotopic ratios are reported in per mil (‰) relative to the Vienna Standard
192 Mean Ocean Water (V-SMOW) international standard for O and Pee Dee Belemnite (V-PDB)
193 standard for C using the conventional δ-notation. For O isotopes, we used the conversion
194 formula: $\delta^{18}O_{SMOW} = 1.03086 \times \delta^{18}O_{PDB} + 30.86$ ‰ (Coplen et al., 1983). Samples and

195 standards were run in duplicate. Results were standardized using an in-house Royal Holloway
196 University of London carbonate standard (RHBNC) calibrated with NBS-19 (marble) and
197 LSVEC (lithium carbonate) international standards. The percentage of carbonate
198 concentration is an estimate comparing peak heights to those of NBS-19 (100 wt% carbonate)
199 and analytical precisions (1SD) were better than ± 0.05‰ for $\delta^{13}C$ and ± 0.1 ‰ for $\delta^{18}O$.

200

201 *3.3.2. Sr isotopes*

202 Strontium isotope analyses of 10 bulk chimney samples were performed by multiple
203 collector-inductively coupled plasma-mass spectrometer (Neptune Plus, Thermo Scientific) at
204 University of the Ryukyus (Japan). The accuracy of $^{87}Sr/^{86}Sr$ measurements was assessed
205 using the international standard SRM-987, yielding an average $^{87}Sr/^{86}Sr$ value of 0.710258 ±
206 0.000023 (2σ, n = 10) in agreement with the reference value of 0.710250 ± 0.000012 (Weis et
207 al., 2005).

208

209 *3.3.3. U-Th isotopes*

210 The chemical procedure for U-Th age dating of chimney samples followed that
211 described in Bayon et al. (2015). About 65 mg of carbonate sample were spiked with a mixed
212 ^{236}U-^{229}Th solution and digested with 7.5 M HNO_3. U and Th fractions were separated by Fe-
213 oxide co-precipitation and conventional anion exchange techniques. U and Th concentrations
214 and isotope ratios were measured with a Thermo Scientific Neptune MC-ICP-MS at the PSO,
215 using a standard-bracketing measurement protocol with IRMM-184 (U) and IRMM036 (Th)
216 reference solutions, respectively. U-Th carbonate age calculation was performed by the
217 isochron method using the ISOPLOT program (Ludwig, 2008) in order to correct measured

Journal Pre-proof

ratios from detrital contamination. The mean isochron age was determined using theoretical end-member at the secular equilibrium (activity ratios = 1.0 ± 0.5).

4. Results

4.1. Petrographical observations and mineralogy

Studied hydrothermal chimneys exhibit a variety of external forms (massive, elongated and bulbous). Many of them correspond to small (≤ 1 m-high), massive and bulbous carbonate chimneys within the depression, while other chimneys correspond to well-developed pinnacles reaching several meters high. Some chimneys are characterized by stromatolitic crusts with crystalline calcite inside the chimneys (Fig. 2). The basement of the chimneys are massive, while the pinnacles are elongated with diameter generally < 5 m. The carbonate chimneys are highly porous and associated with surficial layers of Fe-oxides. At centimeter-scale, dendritic calcite is also observed within these massive chimneys (Fig. 2). X-ray diffractometry (XRD) measurements (not presented here, but available upon request) reveal that surface sediments at the Sakallol depression are composed of halite, quartz, anhydrite, anorthite, microcline, anorthoclase, clinochlore, tremolite and muscovite. In contrast, some chimney samples exhibit only calcite and Mg-calcite while other are dominated by calcite and Mg-calcite, quartz, fluorite and anorthite.

Additionally, the microscopic analysis of thin sections reveals the occurrence of particular chimneys characterized by successive concentric layers of carbonate precipitates intertwined with mixed carbonate-silica deposits filling the porosity between carbonate layers (Fig. 3 A to

I). In fact, the analysis of the spaces between carbonate layers by electron microprobe show evidence of (i) the presence of shell that is made of Ca-carbonate with amorphous silica deposited over it (Fig. 3 A-B-C) and (ii) detrital quartz and aluminosilicate minerals with size around 10 µm (Fig. 3 D to I). Other minerals such us barite, titanomagnetite and iron oxide have been detected in carbonate chimneys.

4.2. Bulk chemical composition

The bulk chemistry of studied chimneys displays significant variability in CaO and SiO_2 abundances, with respective ranges of 2.8 to 54.8 wt %, and 0.7 to 50.9 wt% (Table 1). Some samples exhibit much lower CaO concentrations (< 2 wt %), while other display instead low SiO_2 abundances < 2% (Table 1). The chimneys having high SiO_2 levels are relatively enriched in MgO (4.9 wt %), NaO (7 wt %), Fe_2O_3 (12.1 wt %) and Al_2O_3 (11.6 wt %) (Table 1), while carbonate chimneys also exhibit lower concentrations of Cu, Co, Ni, Zn, V, Co than the mixed carbonate-siliceous chimneys (Table 1).

4.3. Trace elements in leached (authigenic) fraction

The REE composition of studied samples shows significant intra-sample variability (Table 2). All samples are characterized by a negative Ce anomaly (Fig. 4). The total amount of the REE (ΣREE) show variations but most of them display enrichment from the outside to the inside of chimneys. Samples DJ-16 displays the highest abundances in REE.

All leachates display very limited Zr/Hf (39.1 ± 4.0; 1 SD) and Y/Ho (32.4 ± 1.5; 1 SD) variability, both being very similar to average values for typical mid-ocean-ridge and ocean-island basalts (36.6 ± 2.9 and 27.7 ± 2.7, respectively; Jochum et al., 1986) and fine-grained clay-size detrital sediments worldwide (36.9 ± 1.8 and 30.5 ± 1.0; Bayon et al., 2015).

4.4. C, O and Sr isotopic composition

The $\delta^{13}C$ values of chimney samples from Sakallol Depression range from -9.44 to 8.92 ‰ whereas $\delta^{18}O$ values vary between -4.5 to 25.3 ‰ (Table 3; Fig. 5). The average values of $\delta^{13}C$ and $\delta^{18}O$ isotope compositions are 3.3 and 0.5 ‰, respectively. Studied chimney samples display $^{87}Sr/^{86}Sr$ ratios ranging from 0.7049 to 0.7056, with an average value of 0.7051 (Table 3; Fig. 6).

4.5. U-Th isotope dating

Studied chimney samples are characterized by low U concentrations, ranging from 0.12 to 0.56 ppm, except for the two DJ-17 samples showing higher U abundances (2.5-3.1 ppm) (Table 2). Corresponding ($^{234}U/^{238}U$) activity ratios range from 1.188 to 1.517, displaying values substantially higher than seawater composition (1.146 ± 0.003; Robinson et al., 2004). Thorium concentrations and associated isotopic ratios were measured in 10 samples, with ^{232}Th and ^{230}Th ranging from 14 to 203 ppb, and 4.8 and 8.1 ppt, respectively (Table 2). All samples define an isochron-like correlation in a ($^{230}Th/^{232}Th$) vs. ($^{238}U/^{232}Th$) diagram, but plotting above the equiline defining secular equilibrium (plot not shown here). The presence of excess ^{230}Th activity relative to ^{238}U activity in studied chimney samples could possibly

reflect a source of hydrogenous ^{230}Th (Haase-Schramm et al., 2004). However, as it will be discussed below, this hypothesis is not supported by the evidence that corresponding leachates display detrital-like Zr/Hf and Y/Ho ratios, excluding any significant contribution from the surrounding aquatic environment. Instead, excess ^{230}Th activity in studied chimney samples could reflect the presence of detrital material not at secular equilibrium, most likely derived from young basalts in the lake catchment area (Lowenstern et al., 2006). As a consequence, no Th dates could be obtained for the set of studied samples.

5. Discussion

5.1. Mineralogy

The XRD analyses of the Sakallol chimneys show that calcite, Mg-calcite and quartz are the most abundant mineral phases in studied samples. In addition to XRD measurements, the relationship between Sr/Ca and Mg/Ca ratios can also be used to quantitatively estimate the relative proportion of different carbonate mineral phases (aragonite, calcite, low Mg-calcite, high-Mg-carbonates) and bulk detrital fraction hosted in carbonate rocks (Table 4; Bayon et al., 2007; Nothen and Kasten, 2011). In studied samples, Sr/Ca and Mg/Ca ratios range from ~0.007 to 2 and from ~0.7 to 2000. These values are higher than those calculated by Gasse and Fontes (1989) for Lake Asal chimneys, which display Sr/Ca values between 17 and 20 × 10^{-4}. More recently, Dekov et al. (2021) also reported Mg/Ca ratios for Lake Asal carbonate chimneys and concluded that this ratio was controlled by the proportion of hydrothermal *vs* seawater in the lake water. Figure 7 illustrates the Sr/Ca versus Mg/Ca relationship for studied

Sakallol samples and inferred endmember compositions, together with values from other hydrothermal carbonates from Lake Abhé, Lost City (Mid Atlantic ridge) and Lake Tanganyika (East Africa Rift). High Mg/Ca ratios are encountered in Si-rich samples, which are best explained as reflecting the presence of detrital material (Fig. 7). In fact, most studied samples plot on mixing lines between the detrital endmember and calcite or Mg-calcite, respectively. Chimneys characterized by high SiO_2 contents fall along the mixing trend between calcite and bulk detrital fraction, while carbonate chimneys mostly plot along the binary mixing relationship between high-Mg carbonates and calcite end-members. Collectively, these simple mixing relationships between binary end-member components (Fig. 7) suggests that carbonate mineral phases are dominated by calcite (up to 90 wt %) and high Mg-carbonate phases (between 10 to 30 wt %), with minor amounts of aragonite (up to ~5 wt %), while also confirming that studied chimney samples from Sakallol have incorporated substantial amounts of bulk detrital material (between ~6 to 93 wt %).

5.2. Nature of fluids

The mineralogy and geochemistry of studied samples show that both carbonate and mixed carbonate-siliceous chimneys coexist in the Sakallol-Harallol area. Most of the well-known carbonate chimneys in the Afar Rift system are located at Lake Abhé and Lake Asal (Gasse et al., 1978; Dekov et al., 2014; 2021). The Lake Abhé water is hyperalkaline (pH = 10), whereas Lake Asal is mildly acidic (Gasse et al., 1978; Dekov et al., 2014; 2021). The Sakallol-Harallol basin geothermal waters are moderately alkaline (pH = 8.11; Awaleh et al., 2017), with temperatures ranging from 46 to 77°C.

334 The Sr isotopic compositions of the studied chimneys range between 0.7049 and
335 0.7056, much lower than the $^{87}Sr/^{86}Sr$ composition of Late Neogene and Quaternary seawater
336 (>0.709). Measured $^{87}Sr/^{86}Sr$ ratios of Sakallol-Harallol chimneys are consistent with Sr
337 isotope compositions of hot spring waters in this area (0.70365 - 0.70626; Awaleh et al.,
338 2017) and Djibouti basalts (0.70309 - 0.70664; Vidal et al., 1991; Barrat et al., 1993; Deniel
339 et al., 1994; Faure, 2001). More recently, Moussa et al. (2017) investigated Sr isotopes of
340 chalcedony-quartz veins (0.7032 and 0.7072), suggesting that Sr was derived from different
341 sources of fluids, such as magmatic, hydrothermal and seawater.

342 Additionally, the large range of measured $\delta^{13}C$ values further suggests mixing between
343 different types of fluids (Fig. 4). The lighter values are consistent with fluids having a
344 magmatic origin (Field and Fifarek, 1985). Depletion of $\delta^{13}C$ values is similar to isotopic
345 composition of reduced organic carbons although hydrothermal carbonates present also
346 depletion of $\delta^{13}C$ values (Rye and Sawkins, 1974; Ohmoto and Rye, 1979; Field and Fifarek,
347 1985). In the Afar Rift system, the $\delta^{13}C$ composition of carbonate minerals and hydrothermal
348 chimneys has already been discussed previously (Gasse et al., 1985; Fouillac et al., 1989;
349 Moussa et al., 2019; Dekov et al., 2014; 2021; DeMott et al., 2021), documenting a large
350 range of $\delta^{13}C$ values indicative of various sources and mixtures between fluids with
351 distinctive magmatic, meteoric and seawater compositions and evaporation conditions during
352 deposition. Awaleh et al. (2017) also demonstrated the presence of substantial magmatic CO_2
353 inputs in Sakallol-Harallol spring waters. As a consequence, the low $\delta^{13}C$ values measured in
354 studied chimney samples most likely derive from deep-seated magmatic fluids, while the
355 heavier values presumably indicate interactions between superficial fluid sources such as
356 meteoric and seawater (with $\delta^{13}C \sim 0‰$). Additionally, Gasse and Fontes (1989) argued that

357 the Sakallol basin was fed by seawater. More recently, Awaleh et al. (2017) confirmed this
358 hypothesis with B isotopes.

359 Concerning O isotopes, the large $\delta^{18}O$ variability observed in studied samples (-4.5 to
360 25.3 ‰) echoes with those reported for carbonates (hydrothermal calcite) discussed elsewhere
361 (Moussa et al., 2019). In the latter study, the large $\delta^{18}O$ range was interpreted as reflecting the
362 presence of calcite derived from phase separation of liquid and gas involving exsolution of
363 carbon dioxide and steam formation (e.g., boiling condition). Several geothermal sites where
364 calcite has been reported, such as Golden Cross and Waiotapu in New Zealand (Hedenquist
365 and Browne, 1989; Simmons and Christenson, 1994; Simmons et al., 2000), also display
366 carbonate minerals having positive $\delta^{18}O$ compositions suggestive of a CO_2-rich vapor phase.
367 In addition, Fouillac et al. (1989) highlighted the importance of deep CO_2 influx for two deep
368 geothermal boreholes drilled in the Asal Rift with oxygen isotope compositions ranging from
369 +7.8 to 20.4‰ for newly-formed calcite. The $\delta^{18}O$ values of hydrothermal fluids from Lake
370 Abhé (-2.82 and -2.93‰; Dekov et al., 2021) and Sakallol (-3.9‰ to -1.72‰; Awaleh et al.,
371 2017) are also negative. Therefore, we infer that negative $\delta^{18}O$ values can be ascribed to
372 hydrothermal fluids, while more positive values most reflect isotopic exchange induced by
373 contact with colder lake surface water.

374 Based on O, C and Sr isotopes, chimneys investigated at Sakallol-Harallol area display
375 contrasted geochemical composition, hence suggesting that the geochemical composition of
376 the paleo-lake waters from which they were precipitated was different and indicate that
377 magmatic fluids interacted with fluids of surficial origin such as meteoric waters, seawater or
378 brine (Fig. 8).

379

380 *5.3. Origin of chimneys*

381

382 Hydrothermal carbonate chimneys have been described in different geodynamic settings
383 (Barrat et al., 2000; Ludwig et al., 2006; Fouquet et al., 2010; Dekov et al., 2014), but only a
384 few investigations have been dedicated to hydrothermal Si-rich chimneys at spreading ridges
385 or continental rift systems (Herzig et al., 1988; Juniper and Fouquet, 1988; Shanks et al.,
386 2005; Dekov et al., 2015).

387 In comparison, the well-studied hydrothermal carbonate chimneys from the Lost City
388 hydrothermal site (Mid-Atlantic Ridge) form under relatively cool (40 to 60°C) and alkaline
389 (pH 9) fluid conditions set by serpentinization of underlying mantle rocks. The mineral phases
390 composing Lost City chimneys are mostly calcite, aragonite and brucite, with no evidence for
391 any sulfide minerals (Kelly et al., 2001).

392 The Afar Rift system is characterized by a distinctive geological setting compared to
393 Lost City. While hydrothermalism in the Afar Rift is not fed by serpentinization, Lake Abhé
394 also hosts similar Lost City-like hydrothermal carbonate chimneys (Dekov et al., 2014). At
395 Lake Abhé, the structure of the chimneys displays an alternation between calcite and low-Mg
396 calcite. A few silica-rich concentric layers have also been observed (Dekov et al., 2014).

397 In the case of the Sakallol-Harallol chimneys, the concentric layers are very different. In
398 fact, whenever calcite is predominant, detrital quartz coexists with calcite. The precipitation
399 of silica in hydrothermal deposits typically occurs under relatively basic conditions when pH
400 reaches ~9 (Chenevoy and Piboule, 2007). Any change of pH in hydrothermal waters, due to
401 steam loss and/or evaporation is likely to trigger silicification of continental carbonates. Silica
402 supersaturation in fluids, as required for silica precipitation, can be achieved through cooling
403 when fluids reach the surface environment (Bustillo et al., 2010). At the Sakallol-Harallol

area, Awaleh et al. (2017) determined dissolved SiO_2 concentrations (92.7 to 123 mg/L) in the different springs, suggesting that high SiO_2 levels probably originated from the alteration of silicate minerals hosted by basaltic rocks. In hydrothermal deposits, silica precipitation is also controlled by temperature and pressure (Chenevoy and Piboule, 2007). High concentration of silica is reported for high T°C seafloor hydrothermal discharges (Herzig et al., 1988; Stuben et al., 1993; German and Von Damm, 2004). Furthermore, under arid climate, intense evaporation of lake water typically leads to highly alkaline and Si-rich waters from which magadiite can precipitate (Bustillo et al., 2010), although no evidence for such mineral phase has been detected at Sakallol-Harallol.

In this study, the presence of shells embedded within the chimney deposits (Fig. 3 A-B-C, D) testifies of biological activity in the paleo-lake. All the above suggests the occurrence of at least three sources of Si in the chimneys: (i) windblown dust delivered via aeolian transport and incorporated in chimneys upon their formation, as inferred from the presence of detrital quartz in studied thin sections (ii) biogenic silica associated with the presence of diatom silicifiers initially formed in the lake and subsequently incorporated in the carbonate chimneys during their formation; (iii) authigenic silica inherited from the alteration of detrital silicate minerals through sub-surface hydrothermal fluid circulation.

Most of the shale-normalized REE distribution patterns in studied samples display negative Ce anomalies and MREE enrichment; features that contrast with the observed REE signatures in Lake Abhé chimneys, in which highly positive Ce anomalies and HREE enrichments were reported, interpreted as reflecting alkaline lake water conditions (Dekov et al., 2014). In contrast, the REE patterns of the chimneys from Lake Tanganyika in East Africa are characterized by negative Ce anomaly (Barrat et al., 2000). Negative Ce anomalies are ubiquitous characteristics of the marine environment (De Baar et al., 1985; Elderfield 1988;

German et al., 1995), reflecting to a large extent intense scavenging of reactive Ce^{4+} onto sinking particulates under typical oxygenated conditions. On this basis, the presence of negative Ce anomalies could be taken as evidence for the presence of seawater-like conditions in the Sakallol-Harallol basin, hence in marked contrast with evidence based on Sr isotopes and trace element ratios (Zr/Hf and Y/Ho). Alternatively, we propose instead that these negative Ce anomalies most likely reflect the signature of weathered volcanogenic particles. The behavior of REE during basalt alteration has been investigated in previous studies, showing that weathered volcanogenic products are typically associated with development of a pronounced negative Ce anomaly (Price et al., 1991; Prudencio et al., 1995; Martin and McCulloch, 1999). The development of Ce-anomalies during basalt weathering is thought to relate to preferential Ce oxidation and sequestration relative to its neighboured trivalent REE (Prudencio et al., 1995); a process which can result in the development of negative Ce-anomalies in weathering products subsequently formed in soils and exported to river systems (Bayon et al., 2020).

5.4. Stages of formation of the hydrothermal chimneys

As described above, two types of inactive hydrothermal chimneys have been identified in the Sakallol basins; the first one corresponding to carbonate chimneys and the second one to mixed carbonate-siliceous buildups. The distribution of O and C isotopic ratios in studied fossil chimneys has provided evidence that magmatic fluids interacted with surficial fluid sources, such as meteoric or seawater, consistent with evidence based on radiogenic Sr isotopes suggesting that Sr in studied chimneys is, at least partly, derived from the alteration

451 of basalts. On the other hand, trace element geochemical analyses show that chimneys exhibit
452 various chemical characteristics (e.g. Zr/Hf and Y/Ho) typical of detrital material.

453 Combining all the above mineralogical and geochemical evidence, we propose that the
454 carbonate-rich chimneys formed at a time when the paleo-lake was sursaturated in dissolved
455 carbonate, as previously suggested for Lake Asal and Abhé carbonate chimneys (Fontes,
456 1977; Gasse and Street, 1989, Dekov et al., 2014). In contrast to Lake Asal and Abhé,
457 however, a second type of hydrothermal chimneys is documented here in the Sakallol basin,
458 characterized by presence of detrital quartz and other silicate grains between the porosity of
459 carbonate layers. We suggest that this compositional variability reflects marked changes in the
460 geochemical composition of lake waters. We suggest that they could reflect either Si-based
461 biological activity, alteration of silicate minerals, and/or intense evaporation. Earlier work
462 based on stable isotopes suggested that higher evaporation rates occurred when a surface
463 connection was established between Asal and Sakallol (Gasse and Fontes, 1989). In fact,
464 under arid climate, intense evaporation could possibly drive a change of lake water chemistry
465 from Ca-bicarbonate to Na-bicarbonate and more alkaline conditions. When the concentration
466 of Ca and Mg decreases during evaporation, the alkalinity, pH, Na and K increase in the lake
467 water. Under today's arid conditions, the springs and boreholes of Sakallol basins are
468 dominated by Na-bicarbonate and Na-chloride.

469 In addition, the presence of young basalt flows in the lake basin could have also released, via
470 chemical weathering under warm and humid conditions, substantial amounts of dissolved Si
471 in the lake water. This would be in a good agreement with the above mentioned evidence for
472 ^{230}Th excess and the fact that $^{87}Sr/^{86}Sr$ ratios point towards a basaltic signature and that Zr/Hf
473 and Y/Ho ratios reflect a detrital origin. Additional geochemical data, in particular the use of
474 proxies for chemical weathering of silicate rocks, would be required however to test these

different hypotheses. Nevertheless, the presence of distinctive hydrothermal deposits at the Allols basin clearly suggests that the corresponding paleo-lake experienced significant geochemical variability through time. Following previous inferences that the Gaggadé-Der Ela grabens and associated sediment deposits (around 40 km of Allols basins) experienced several major tectonic and climatic fluctuations during the Plio-Pleistocene period (Gasse et al., 1980), we describe below a possible scenario accounting for the precipitation of the chimneys in the Allols basin:

(i) The formation of the carbonate chimneys corresponds to a wet period during which the paleo-lake was saturated with carbonate, resulting in calcite and Mg-carbonate precipitation, most likely during the humid Mid-Holocene period.

(ii) Followed the onset of arid conditions, presumably at the end of the African Humid period (from ca. 5 kyr B.P.), a compositional change of the lake water chemistry, towards higher dissolved silica concentrations, due possibly to more intense aeolian activity followed by subsequent dissolution in the lake water column, drove precipitation of mixed carbonate-siliceous chimneys and/or diagenetic replacement of previously formed carbonate chimneys. To some extent, this latter type of mixed carbonate-silica chimneys resembles unusual laminated authigenic carbonate chimneys from the Makran margin (Arabian Sea) where the alternation of authigenic (methane-derived) carbonate and detrital Si-rich layers has been found to reflect changing aeolian fluxes of windblown detrital particles to overlying surface waters (Himmler et al., 2016).

Journal Pre-proof

Journal Pre-proof

6. Conclusions

Both carbonate and mixed carbonate-siliceous hydrothermal chimneys are reported at the Sakallol depression. Mineralogical and geochemical analyses of these chimneys show that calcite, Mg-calcite and detrital material (quartz) are the most abundant mineral phases in studied samples. The REE distribution patterns of studied samples display negative Ce anomalies; a feature which we interpret here as reflecting the presence of colloidal detrital particles related to weathering of surrounding basalts. This hypothesis is reinforced by other geochemical indices, such as radiogenic Sr isotopes, and Zr/Hf and Y/Ho ratios, which collectively indicate that the chemistry of these chimneys is strongly influenced by silicate detritus.

Additionally, the studied chimneys display contrasted geochemical compositions for O and C isotopes, suggesting that the chemistry of the paleo-lake waters from which they were precipitated was also influenced by magmatic fluid interacting with superficial fluid sources such as meteoric and seawater or brine.

Overall, these findings are used to propose a two-stage conceptual model for the formation of Sakallol chimneys. The first stage corresponds to the precipitation of carbonate chimneys under wet climate and high lake level conditions, while the second stage of formation was related to the deposition of detrital quartz (perhaps associated with precipitation of authigenic silica) under more arid conditions, when lake water chemistry became influenced by enhanced silica enrichment due to dissolution of aeolian dust.

Journal Pre-proof

Acknowledgements

This research was supported by the CERD (Center for Research and Studies of Djibouti). The authors are warmly grateful to Dr. J. Mohamed for all his support during this research. We are also grateful to the Djiboutian Army for all their efforts to facilitate our sampling campaigns at Sakallol depression. We also greatly acknowledge the Editor (Prof. Damien Delvaux) and reviewers, for providing insightful and constructive comments.

Journal Pre-proof

References

Alonso-Zarza, A.M., Genise, J.F., Verde, M., (2011). Sedimentology, diagenesis and ichnology of Cretaceous and Palaeogene calcretes and palustrine carbonates from Uruguay. Sedimentary Geology, 236 (1–2), 45-61.

Audin, L., Manighetti, I., Tapponnier, P., Metivier, F., Jacques, E., Huchon, P., (2001). Fault propagation and climatic control of sedimentation on the Ghoubbet rift floor: Insights from the Tadjouraden cruise in the Western Gulf of Aden. Geophys. J. Int., 144, 391-413.

Awaleh, M.O., Hoch, F.B., Boschetti, T., Soubaneh, Y.D., Egueh, N.M., Elmi, S.A., Jalludin, M., Khaireh, M.A., (2015a). The geothermal resources of the Republic of Djibouti – II: geochemical study of the Lake Abhe geothermal field. J. Geochem. Explor. 159, 129-147.

Awaleh, M.O., Hoch, F.B., Kadieh, I.H., Soubaneh, Y.D., Egueh, N.M., Jalludin, M., Boschetti, T., (2015b). The geothermal resources of the Republic of Djibouti – I: hydro geochemistry of the Obock coastal hot springs. J. Geochem. Explor. 152, 54-66.

Awaleh, M.O., Boschetti, T., Soubaneh, Y.D., Baudron, P., Kawalieh, A.D., Dabar, O.A., Ahmed, M.M., Ahmed, S.I., Daoud, M.A., Egueh, N.M., Jalludin, M., (2017a). Geochemical study of the Sakalol – Harralol geothermal field (Republic of Djibouti): evidences of a low enthalpy aquifer between Manda-Inakir and Asal rift settings. J. Volcanol. Geotherm. Res. 331, 26-52.

Barberi, F., Borsi, S., Ferrara, G., Marinelli, G., Varet, J., (1970). Relations between tectonic and magmatology in the northern Danakil Depression (Ethiopia). Philos. Trans. R. Sot. London, Ser. A, 267, 293-311.

Barberi, F., Varet, J., (1977). Volcanism of Afar: Small-scale plate tectonics implications. Geological Society of America Bulletin 88, 1251-1266.

Barrat, J.A., Jahn, B.M., Fourcade, S., Joron, J.L., (1993). Magma genesis in an ongoing rifting zone: the Tadjoura Gulf (Afar area). Geochim. Cosmochim. Acta 57, 2291-2302.

Barrat, J.A., Bayon, G., Wang, X., Le Goff, S., Rouget, M.L., Gueguen, B., Salem, D.B. (2020). A new chemical separation procedure for the determination of rare earth elements and yttrium abundances in carbonates by ICP-MS. Talanta 219, 121244.

Barrat, J.A., Keller, F., Amossé, J., Taylor, R.N., Nesbitt, R.W., Hirata, T., (1996). Determination of rare earth elements in sixteen silicate reference samples by ICP-MS after Tm addition and ion exchange separation. Geostandards Newsletter 20(1), 133-139.

Bayon, G., Douglas, G.B., Denton, G.J., Monin, L., De Deckker, P., (2020). Preferential riverine export of fine volcanogenic particles to the Southeast Australian margin. Frontiers in Marine Science 7, 89.

Bayon, G., Henderson, G.M., Etoubleau, J., Caprais, J.C., Ruffine, L., Marsset, T., Sultan, N., 2015. U-Th isotope constraints on gas hydrate and pockmark dynamics at the Niger delta margin. Marine Geology 370, 87-98.

Bayon, G., Pierre, C., Etoubleau, J., Voisset, M., Cauquil, E., Marsset, T., Fouquet, Y., (2007). Sr/Ca and Mg/Ca ratios in Niger Delta sediments: implications for authigenic carbonate genesis in cold seep environments. Marine Geology 241(1-4), 93-109.

Bustillo, M.A., 2010. Silicification of continental carbonates. Developments in Sedimentology, 62, 153-178.

Chenevoy M.., Piboule M., (2007). Hydrothermalisme : Spéciation métallique hydrique et systèmes hydrothermaux. Edt. EDP Sciences.

593 Coplen, T. B., Kendall, C., & Hopple, J. (1983). Comparison of stable isotope reference
594 samples. *Nature*, *302*(5905), 236-238.
595 Daoud, M.A., Le Gall, B., Maury, R.C., Rolet, J., Huchon, P., (2011). Young rift kinematics
596 in the Tadjoura rift, western Gulf of Aden. Tectonics, 30, TC1002,
597 doi:10.1029/2009TC002614.
598 D'Amore, F., Giusti, D., Abdallah, A., (1998). Geochemistry of the high salinity geothermal
599 field of Asal, Republic of Djibouti Africa. Geothermics 27, 197-210.
600 De Chabalier JB, Avouac JP (1994) Kinematics of the Asal Rift (Djibouti) determined from
601 the deformation of Fieale Volcano. Science 265:1677–168
602 DeMott, L.M., Scholz, C.A., Awaleh, M.O., (2021). Lacustrine carbonate towers of Lake
603 Abhe, Djibouti: Interplay of hydrologic and microbial processes. Sedimentary Geology
604 424, 105983.
605 Dekov, V.M., Egueh, N.M., Kamenov, G.D., Bayon, G., Lalonde, S.V., Schmidt, M.,
606 Liebetrau, V., Munnik, F., Fouquet, Y., Tanimizu, M., Awaleh, M.O., Farah, I.G., Le
607 Gall, B., (2014). Hydrothermal carbonate chimneys from a continental rift (Afar Rift):
608 mineralogy, geochemistry and mode of formation. Chem. Geol. 387, 87-100.
609 Dekov, V.M, Lalonde, S.V, Kamenov, G.D, Bayon, G., Shanks III, W.C., Fortin, D., Fouquet,
610 Y., Moscati, R.J., (2015). Geochemical and Mineralogy of silica chimneys from an
611 inactive seafloor hydrothermal field (East Pacific Rise, 18°S). Chem. Geol. 415, 126-
612 140.
613 Dekov, V.M., Guéguen, B., Yamanaka, T., Moussa, N., Okumura, T., Bayon, G., Liebetrau,
614 V., Yoshimura, T., Kamenov, G., Araoka, D., Makita, H., Sutton, J., (2021). When a
615 mid-ocean ridge encroaches a continent: Seafloor-type hydrothermal activity in Lake
616 Asal (Afar Rift). Chemical Geology 568, 120126.
617 Deniel, C., Vidal, P., Coulon, C., Vellutini, P.J., Piguet, P., (1994). Temporal evolution of
618 mantle sources during continental rifting: the volcanism of Djibouti (Afar). J. Geophys.
619 Res. 99, 2853-2869.
620 Doubre, C., Manighetti, I., Dorbath, C., Dorbath, L., Bertil, D., Delmond, J.C., (2007).
621 Crustal structure and magmato-tectonic processes in an active rift (Asal–Ghoubbet,
622 Afar, East Africa): Insights from the 23-year recording of seismicity since the last
623 rifting event. Journal of Geophysical Research 112, B05406.
624 Dugda, M.T., Nyblade, A.A., (2006). New constraints on crustal structure in eastern Afar
625 from the analysis of receiver functions and surface waves dispersion in Djibouti. In:
626 Yirgu, G., Ebinger, C.J., Maguire, P.K. (Eds), The Afar Volcanic Province within the
627 East African Rift System. Geological Society, London, Special Publications 259, 239-
628 251.
629 Faure, G., (2001). Origin of Igneous Rocks: The Isotopic Evidence. Springer-Verlag, Berlin
630 Heidelberg GmbH.
631 Field, C.W., Fifarek, R.H., (1985). Light stable isotope systematics in epithermal systems.
632 Rev. Econ. Geology 2, 99-128.
633 Fontes, J.C., Edmunds, W.M., (1989). The Use of Environmental Isotope Techniques in Arid
634 Zone Hydrology - a Critical Review. IHP-III Project 5.2, Document Code: SC/89/
635 WS/33. Unesco, Paris.
636 Fouillac, A., Fouillac, C., Cesbron, F., Pillard, F., Legendre, O., (1989). Water-rock
637 interaction between basalt and high-salinity fluids in the Asal Rift, Republic of Djibouti.
638 Chem. Geol. 76, 271–289.
639

640 Fouquet, Y., Cambon, P., Etoubleau, J., Charlou, J.L., Ondréas, H., Barriga, F.J.A.S.,
641 Cherkashov, G., Semkova, T., Poroshina, I., Bohn, M., Donval, J.P., Henry, K.,
642 Murphy, P., Rouxel, O., (2010). Geodiversity of hydrothermal processes along the Mid-
643 Atlantic Ridge and ultramafic-hosted mineralization: a new type of oceanic Cu-Zn-Co-
644 Au volcanogenic massive sulfide deposit. In: Rona, P.A., Devey, C.W., Dyment, J.,
645 Murton, B.J. (Eds.), Diversity of Hydrothermal Systems on Slow Spreading Ocean
646 Ridges. Geophysical Monograph 188, pp. 321-367
647 Gasse, F., (1975). L'évolution des lacs de l'Afar central (Ethiopie et T.F.A.I.) du Plio-
648 Pléistocène à l'Actuel. Thesis. Univ. Paris VI, Paris, 390 pp.
649 Gasse, E., & Street, F. A. (1978). Late Quaternary lake-level fluctuations and environments of
650 the northern Rift Valley and Afar region (Ethiopia and Djibouti). Palaeogeography,
651 Palaeoclimatology, Palaeoecology, 24(4), 279-325.
652 Gasse, F., Varet, J., Mazet, G., Recroix, F., & Ruegg, J. C. (1986). Carte géologique de la
653 République de Djibouti: feuille de Eali Sabieh, Ministère Français des Relations
654 Extérieures et ISERST, 1/100000. ORSTOM Ed
655 Gasse, F., Fontes, J.C., (1989). Paleoenvironments and paleohydrology of a tropical closed
656 lake (Lake Asal, Djibouti) since 10 000 yrs BP. Paleogeogr, Paleoclimatol, Paleoecol
657 69, 67-102.
658 German, C.R., and K.L. Von Damm., (2004). Hydrothermal processes. Pp. 181–222 in
659 Treatise on Geochemistry, Volume 6: The Oceans and Marine Geochemistry. H.D.
660 Holland and K.K. Turekian, eds, Elsevier, London
661 Haase-Schramm, A., Goldstein, S.L. and Stein, M., (2004). U-Th dating of Lake Lisan
662 aragonite (late Pleistocene Dead Sea) and implications for glacial East Mediterranean
663 climate change. Geochim. Cosmochim. Acta 68, 985-1005
664 Hammond, J.O., Kendall, J.M., Stuart, G.W., Keir, J., Ebinger, C.J., Ayele, A., Belachew, M.,
665 (2011). The nature of the crust beneath the Afar triple junction: Evidence from receiver
666 functions. Geochemistry, Geophysics, Geosystems, 12, Q12004.
667 Hedenquist, J.W., Browne, P.R., (1989). The evolution of the Waiotapu geothermal system,
668 New Zealand, based on the chemical and isotopic composition of its fluids, minerals
669 and rocks. Geochim. Cosmochim. Acta 53 (9), 2235–2257.
670 Herzig, P.M., Becker, K.P., Stoffers, P., Bäcker, H., Blum, N., (1988). Hydrothermal silica
671 chimney fields in the Galapagos Spreading Center at 86°W. Earth Planet. Sci. Lett. 89,
672 261-272.
673 Himmler, T., Bayon G., Wangner D., Enzmann F., Peckmann J., Bohrmann G., (2016) Seep-
674 carbonate lamination controlled by cyclic particle flux. *Sci. Rep.* **6**, 37439; doi:
675 10.1038/srep37439 Jochum, K. P., Seufert, H. M., Spettel, B., & Palme, H. (1986). The
676 solar-system abundances of Nb, Ta, and Y, and the relative abundances of refractory
677 lithophile elements in differentiated planetary bodies. Geochimica et Cosmochimica
678 Acta, *50*(6), 1173-1183
679 Juniper, S.K., Fouquet, Y., (1988). Filamentous iron-silica deposits from modern and ancient
680 hydrothermal sites. Can. Mineral. 26, 859-869.
681 Kelley, D. S., et al. (2001), An off-axis hydrothermal vent field near the Mid-Atlantic Ridge
682 at 30° N, Nature, 412(6843), 145–149.
683 Le Gall, B., Daoud, M.A., Maury, R.C., Rolet, J., Guillou, H., Sue, C., (2010). Magma-driven
684 antiform structures in the Afar rift: the Ali Sabieh range, Djibouti. J. Struct. Geol. 32,
685 843-854.
686 Lowenstern, J.B., Charlier, B.L.A., Clynne, M.A., and Wooden, J.L., (2006). Extreme U-Th
687 disequilibrium in rift-related basalts, rhyolites and granophyric granite and the timescale

of rhyolite generation, intrusion and crystallization at the Alid volcanic center, Eritrea: Journal of Petrology, v. 47, no. 11, p. 2105-2122.

Ludwig, K.R., (2008). Using Isoplot/Ex, Version 3.70. A geochronological toolkit for Microsoft Excel: Berkeley Geochronology Ctr. Spec. Pub. 4.

Nöthen, K., Kasten, S., (2011). Reconstructing changes in seep activity by means of pore water and solid phase Sr/Ca and Mg/Ca ratios in pockmark sediments of the Northern Congo Fan. Marine Geology 287(1-4), 1-13.

Nozaki, Y., Zhang, J., Amakawa, H., (1997). The fractionation between Y and Ho in the marine environment. Earth and Planetary Science Letters 148(1-2), 329-340

Manighetti, I., Tapponnier, P., Gillot, P.Y., Jacques, E., Courtillot, V., Armijo, R., Ruegg, J.-C., King, G., (1998). Propagation of rifting along the Arabia-Somalia plate boundary: Into Afar. J. Geophys. Res. 103, 4947-4974.

Martin, C. E., and McCulloch, M. T. (1999). Nd-Sr isotopic and trace element geochemistry of river sediments and soils in a fertilized Catchment, New South Wales, Australia. Geochim. Cosmochim. Acta 63, 287–305.

McCrea, J. M. (1950). On the isotopic chemistry of carbonates and a paleotemperature scale. The Journal of Chemical Physics, 18(6), 849-857.

Moussa N., Boiron M.C., Grassineau N., Asael D., Fouquet Y., Le Gall B., Etoubleau J., Rolet J., Delacourt C., (2019). Mineralogy, fluid inclusion and stable isotopes studies of Epithermal Au-Ag-Bi-Te mineralization from the SE Afar Rift (Djibouti). Ore Geology Reviews. 111, 102916, 1-14.

Moussa, N., Rouxel, O., Grassineau, N.V., Ponzevera, E., Nonnotte, P., Fouquet, Y., Le Gall, B., (2017). Sulfur and strontium isotopic study of epithermal mineralization: a case study from the SE Afar Rift Djibouti. Ore Geol. Rev. 81, 358-368.

Ohmoto, H., Rye, R.O., 1979. Isotopes of Sulfur and Carbon. In: Barnes, H.L. (Ed.), Geochemistry of Hydrothermal Ore Deposits, second ed. Wiley, New York, pp. 509-567.

Pinzutti, P., Humler, E., Manighetti, I., Gaudemer, Y., (2013). Petrological constraints on melt generation beneath the Asal rift, Djibouti using Quaternary basalts. Geochemistry, Geophysics, Geosystems 14, 2932-2953.

Pouchou LJ, Pichoir F (1984) New model quantitative x-ray microanalysis. Application to the analysis of homogeneous samples. Recherche Aerospatiale 3:13–38

Pourmand, A., Dauphas, N., Ireland, T.J., 2012. A novel extraction chromatography and MC-ICP-MS technique for rapid analysis of REE, Sc and Y: Revising CI-chondrite and Post-Archean Australian Shale (PAAS) abundances. Chemical Geology 291, 38-54.

Price, R. C., Gray, C. M., Wilson, R. E., Frey, F. A., and Taylor, S. R., (1991). The effects of weathering on rare-earth element, Y and Ba abundances in Tertiary basalts from southeastern Australia. Chem. Geol. 93, 245–265.

Prudêncio, M. I., Gouveia, M. A., and Braga, M. S., (1995). REE distribution in present-day and ancient surface environments of basaltic rocks (central Portugal). Clay Miner. 30, 239–248. doi: 10.1180/claymin.1995.030.3.07

Robinson, L. F., N. S. Belshaw, and G. M. Henderson, (2004). U and Th concentrations and isotope ratios in modern carbonates and waters from the Bahamas, Geochem. Cosmochim. Acta, 68(8), 1777– 1789.

Rona, P.A., (1984). Hydrothermal mineralization at seafloor spreading centers. Earth Sci. Rev. 20(1), 1-104.

Rye, R.O., Sawkins, F., (1974). Fluid inclusion and stable isotope studies on the Casapalca Ag-Pb-Zn-Cu deposit, central Andes, Peru. Econ. Geol 69(2), 181-205.

Shanks III, W.C., Morgan, L.A., Balistrieri, L., Alt, J., 2005. Hydrothermal vent fluids, siliceous hydrothermal deposits, and hydrothermally altered sediments in Yellowstone Lake. In: Inskeep, W.P., McDermott, T.R. (Eds.), Geothermal Biology and Geochemistry in Yellowstone National Park. Proceedings of the Thermal Biology Institute workshop, Yellowstone National Park, October (2003). Montana State University Press, Bozeman, MT, pp. 53-72.

Simmons, S.F., Arehart, G., Simpson, M.P., Mauk, J.L., (2000). Golden Cross Low-Sulfidation, Epithermal Au-Ag Deposit. New Zealand. Econ. Geol. 95, 99–112.

Simmons, S.F., Christenson, B.W., (1994). Origins of calcite in a boiling geothermal system. Amer. J. Sci. 294, 361.

Tanaka, Y., Hirata, T., (2018). Stable isotope composition of metal elements in biological samples as tracers for element metabolism. Analytical Sciences 34, 645-655.

Taylor, S.R., McLennan, S.M., 1985. The Continental Crust: Its Composition and Evolution. Blackwell, Oxford, (311 pp.).

Sanjuan, B., Michard, G., Michard, A., (1990). Origine des substances dissoutes dans les eaux des sources thermales et des forages de la région Asal-Ghoubbet (République de Djibouti). J. Volcanol. Geotherm. Res. 43 (1), 333-352.

Stietljes, L., (1973). L'axe tectono-volcanique d'Asal (Afar central-Territoire français des Afars et des Issas).Thesis, Université de Paris-Sud, Orsay.

Vellutini, P., 1990. The Manda-lnakir Rift, Republic of Djibouti: a comparison with the Asal. Rift and its geodynamic interpretation. Tectonophysics 172, 141-153.

Vidal, P., Deniel, C., Vellutini, P.J., Piguet, P., Coulon, C., Vincent, J., Audin, J., (1991). Changes of mantle source in the course of a rift evolution: the Afar case. Geophys. Res. Lett. 18, 1913-1916.

Weis, D., Kieffer, B., Maerschalk, C., Pretorius, W., & Barling, J. (2005). High-precision Pb-Sr-Nd-Hf isotopic characterization of USGS BHVO-1 and BHVO-2 reference materials. Geochemistry, Geophysics, Geosystems, 6(2)

Journal Pre-proof

Figure captions:

Figure 1. A: Schematic geological map of the Republic of Djibouti (SE Afar Rift) after Vellutini and Piquet (1994); B: Geological map of the Sakallol basins (studied areas); C-D: Photographs of the Sakallol basins (C: Haralé plain, D: The red line corresponds to an example of travertine).

Figure 2. Types of chimneys observed in the Sakallol basins: elongated (A, B, C); massive (D, F, G); dendritic (G) and stromatolitic crust and crystalline structures (E).

Figure 3. Cross-sections of chimneys: (A) sample of a carbonate chimney; (B-C) X-ray maps in Si *K*α (B) and Ca *K*α (C) lines showing the presence of shell that is made of Ca-carbonate with amorphous silica deposited over it; (D) quartz grains within the pore space of chimney carbonate matrix; (E – I) back-scattered electrons image (E) and X-ray maps (F – in Al *K*α, G – Ca *K*α, H – Mg *K*α, and I – Si *K*α lines) showing presence of detrital aluminosilicate grains within the pore space of chimney carbonate matrix.

Figure 4. Post-Archean Australian Shale (PAAS)-normalized (Taylor and McLennan, 1985) REE patterns of the studied samples. Each sample is represented by line with the same color. The different layers (≠L) correspond to the layers from the inner towards the outers of each sample.

Figure 5. Carbon ($\delta^{13}C$) and oxygen ($\delta^{18}O$) isotope compositions of the studied samples.

Figure 6. Strontium isotope composition ($^{87}Sr/^{86}Sr$) of the Sakallol chimneys compared to that of the Lake Asal and Lake Abhé chimneys (Dekov et al., 2014; 2021).

Figure 7. Correlation between Sr/Ca and Mg/Ca (wt ratio) of carbonate chimneys (this study) and carbonates from other studies (Ludwig et al., 2006; Bayon et al., 2007; Dekov et al., 2014; 2021).

Figure 8. Schematic model of the studied area, which shows the relation between the Sakallol basins hydrothermal precipitation, groundwater and seawater from the Ghoubbet al-Kharab (Not at scale).

Table 1: Results of the analysis of samples from the Allols basins.

Journal Pre-proof

Table 2: Chemical composition of the chimneys. Trace elements are in ppm.

Table 3: Carbon, oxygen and strontium isotope values of the samples from the Allols basins.

Table 4: Sr/Ca and Mg/Ca of end-member components (values of aragonite - high-Mg calcite; biogenic calcite and detrital fraction are from Bayon et al., 2007)

Journal Pre-proof

Journal Pre-proof

Samples	SiO_2 (%)	Al_2O_3 (%)	FeO (%)	MgO (%)	CaO (%)	Na_2O (%)	K_2O (%)	TiO_2 (%)	P_2O_5 (%)	MnO (%)	Total (%)	Ba (ppm)	Co (ppm)	Cu (ppm)	Ni (ppm)	Sc (ppm)	Sr (ppm)	V (ppm)	Zn (ppm)
DJ-SK-01-15*	31.4	8.8	7.9	3.9	18.5	7.1	0.7	1.78	0.19	0.11	80.31	114.3	27.4	58.4	43.7	21.1	316.4	231.3	75.4
DJ-SK-04-15*	38.9	10.8	7.1	4.9	11.5	4.1	1.7	1.11	0.22	0.12	80.46	359.9	21.9	63.4	64.7	16.2	417.4	154.8	84.4
DJ-SK-05-15**	50.9	8.5	6.1	2.4	2.8	9.7	1.7	1.36	0.16	0.06	83.66	171.0	19.5	42.8	34.9	14.4	136.9	123.7	49.3
DJ-SK-06-15*	1.4	0.1	0.0	1.2	53.7	0.3	0.0	0.01	0.00	0.01	56.78	69.9	1.7	2.8	5.5	0.7	1353.4	0.1	47.6
DJ-SK-07-15*	5.6	0.5	0.5	2.3	49.9	0.3	0.1	0.11	0.04	0.02	59.31	53.6	3.3	4.8	6.3	1.1	1265.5	19.3	42.1
DJ-SK-08-15*	0.8	0.1	0.1	0.8	54.8	0.2	0.0	0.02	0.00	0.01	56.72	37.5	3.6	7.8	8.1	0.2	889.6	0.1	39.2
DJ-SK-09-15*	5.8	1.3	1.4	1.7	49.1	0.4	0.2	0.34	0.07	0.03	60.21	103.4	1.6	12.9	19.9	2.7	1006.5	43.2	118.9
DJ-SK-10-15*	0.7	0.0	0.0	1.1	53.1	0.3	0.0	0.01	0.00	0.01	55.20	40.5	0.2	1.1	4.0	0.0	1308.8	3.2	37.1
DJ-SK-11-15*	11.6	0.7	0.4	3.3	44.2	0.4	0.1	0.06	0.02	0.01	60.79	112.2	4.1	6.2	13.0	1.1	591.6	4.2	36.9
DJ-SK-12-15*	43.1	11.6	12.1	4.6	12.2	3.1	0.9	2.93	0.58	0.18	91.27	256.0	44.5	76.9	27.8	25.5	448.8	294.8	109.4
DJ-SK-13A-15*	1.0	0.1	0.1	0.9	54.5	0.2	0.0	0.01	0.00	0.01	56.77	42.4	0.3	2.3	1.0	0.2	815.4	2.1	84.0
DJ-SK-13B-15*	12.5	2.1	1.5	5.5	33.6	6.0	0.7	0.25	0.09	0.03	62.35	143.5	4.9	33.3	20.1	3.3	830.2	57.4	42.5
DJ-SK-14A-15**	3.5	0.8	0.6	0.8	51.3	0.4	0.1	0.12	0.03	0.05	57.66	1099	3.7	14.0	12.3	1.6	1309.4	16.4	50.4
DJ-SK-14B-15**	31.7	0.5	0.4	0.3	38.1	0.3	0.1	0.05	0.05	0.09	71.70	105.4	3.0	44.6	14.2	0.8	409.3	23.9	34.8
DJ-SK-15-15*	1.3	0.2	0.2	0.6	53.9	0.5	0.0	0.04	0.02	0.02	56.91	58.0	0.0	0.4	9.6	0.8	627.1	8.3	39.9
DJ-SK-16-15 *	2.7	0.3	0.3	1.1	52.7	0.3	0.0	0.06	0.00	0.02	57.64	208.0	3.2	4.7	15.2	0.5	1528.4	7.7	46.2

Tab. 1

Journal Pre-proof

Journal Pre-proof

	DJ-SK-5-L1-15	DJ-SK-5-L2-15	DJ-SK-06-L1-15	DJ-SK-06-L2-15	DJ-SK-07-L1-15	DJ-SK-07-L2-15	DJ-SK-07-L3-15	DJ-SK-13-L1-15	DJ-SK-13-L2-15	DJ-SK-13-L3-15	DJ-SK15-L1-15	DJ-SK-16-L1-15	DJ-SK-16-L2-15	DJ-SK-16-L3-15	DJ-SK-16-L4-15	DJ-SK-17-L1-15	DJ-SK-17-L2-15
Hf	*0.028*	*0.024*	*0.018*	*0.003*	*0.017*	*0.013*	*0.012*	*0.031*	*0.008*	*0.003*	*0.010*	*0.029*	*0.043*	*0.021*	*0.030*	*0.005*	*0.008*
Y	*1.430*	*1.453*	*0.921*	*0.619*	*1.186*	*0.948*	*0.960*	*0.890*	*0.400*	*0.575*	*0.981*	*1.437*	*1.815*	*1.183*	*1.079*	*0.400*	*0.346*
La	*0.990*	*1.089*	*0.666*	*0.424*	*0.806*	*0.638*	*0.693*	*0.687*	*0.277*	*0.334*	*0.724*	*1.035*	*1.332*	*0.848*	*0.770*	*0.211*	*0.320*
Ce	*1.615*	*1.702*	*1.156*	*0.518*	*0.983*	*0.777*	*1.003*	*1.152*	*0.384*	*0.219*	*0.919*	*1.590*	*2.266*	*1.126*	*1.240*	*0.442*	*0.706*
Pr	*0.257*	*0.283*	*0.174*	*0.105*	*0.202*	*0.163*	*0.182*	*0.179*	*0.069*	*0.072*	*0.174*	*0.263*	*0.342*	*0.206*	*0.178*	*0.051*	*0.075*
Nd	*1.084*	*1.186*	*0.732*	*0.451*	*0.853*	*0.684*	*0.768*	*0.745*	*0.282*	*0.315*	*0.732*	*1.110*	*1.426*	*0.860*	*0.749*	*0.215*	*0.303*
Sm	*0.234*	*0.252*	*0.154*	*0.089*	*0.182*	*0.145*	*0.162*	*0.152*	*0.059*	*0.062*	*0.149*	*0.235*	*0.302*	*0.178*	*0.157*	*0.042*	*0.059*
Eu	*0.055*	*0.059*	*0.033*	*0.015*	*0.037*	*0.030*	*0.033*	*0.028*	*0.009*	*0.010*	*0.024*	*0.053*	*0.064*	*0.038*	*0.033*	*0.010*	*0.013*
Tb	*0.036*	*0.038*	*0.024*	*0.014*	*0.028*	*0.022*	*0.024*	*0.023*	*0.008*	*0.010*	*0.023*	*0.036*	*0.045*	*0.028*	*0.025*	*0.007*	*0.008*
Dy	*0.219*	*0.229*	*0.144*	*0.089*	*0.174*	*0.139*	*0.151*	*0.142*	*0.057*	*0.076*	*0.149*	*0.222*	*0.273*	*0.165*	*0.151*	*0.049*	*0.053*
Ho	*0.045*	*0.047*	*0.030*	*0.018*	*0.036*	*0.029*	*0.030*	*0.029*	*0.013*	*0.017*	*0.032*	*0.046*	*0.056*	*0.034*	*0.032*	*0.011*	*0.011*
Er	*0.120*	*0.121*	*0.079*	*0.048*	*0.096*	*0.076*	*0.077*	*0.079*	*0.034*	*0.048*	*0.084*	*0.119*	*0.147*	*0.091*	*0.086*	*0.031*	*0.028*
Yb	*0.092*	*0.093*	*0.058*	*0.028*	*0.059*	*0.046*	*0.051*	*0.062*	*0.022*	*0.030*	*0.057*	*0.089*	*0.109*	*0.065*	*0.070*	*0.029*	*0.025*
Lu	*0.013*	*0.012*	*0.008*	*0.004*	*0.008*	*0.006*	*0.007*	*0.009*	*0.003*	*0.003*	*0.008*	*0.012*	*0.015*	*0.009*	*0.010*	*0.004*	*0.003*
ΣREE	0.396	0.417	0.259	0.146	0.296	0.236	0.258	0.258	0.098	0.118	0.254	0.397	0.498	0.299	0.279	0.091	0.104

Tab. 2:

Journal Pre-proof

Journal Pre-proof

To be continued

	Sr	Y	Zr	Nb	Mo	Cs	Ba	Hf	U	Sc	V	Mn	Co	Ni	Cu	Rb
DJ SK-5-CI-1_5K	*498*	*1.430*	*1.119*	*0.025*	*0.494*	*0.024*	*45.973*	*0.028*	*0.138*	*0.186*	*3.550*	*79.006*	*0.632*	*1.379*	*4.052*	*0.819*
DJ-SK-5-CI-2_5K	*499*	*1.453*	*0.872*	*0.026*	*0.575*	*0.022*	*47.690*	*0.024*	*0.106*	*0.170*	*2.574*	*90.346*	*0.554*	*1.185*	*2.402*	*0.858*
DJ-SK-06-1	*1128*	*0.921*	*0.851*	*0.056*	*0.921*	*0.048*	*53.144*	*0.018*	*0.455*	*0.068*	*9.637*	*89.606*	*0.561*	*0.546*	*2.989*	*1.419*
DJ-SK-06-2	*1284*	*0.619*	*0.169*	*0.012*	*1.246*	*0.019*	*63.558*	*0.003*	*0.204*	*0.029*	*1.366*	*59.441*	*0.640*	*0.117*	*13.216*	*0.387*
DJ-SK-07-1	*1347*	*1.186*	*0.693*	*0.037*	*0.674*	*0.030*	*47.799*	*0.017*	*0.200*	*0.070*	*2.301*	*116.693*	*0.374*	*0.393*	*8.538*	*0.863*
DJ-SK-07-2	*1436*	*0.948*	*0.498*	*0.028*	*0.472*	*0.027*	*44.641*	*0.013*	*0.200*	*0.048*	*2.197*	*103.792*	*0.247*	*0.175*	*5.346*	*0.665*
DJ-SK-07-3	*1478*	*0.960*	*0.493*	*0.025*	*0.471*	*0.023*	*43.981*	*0.012*	*0.197*	*0.058*	*1.701*	*65.617*	*0.236*	*0.215*	*3.235*	*0.631*
DJ-SK-13-1	*545*	*0.890*	*1.283*	*0.059*	*1.727*	*0.027*	*91.679*	*0.031*	*0.331*	*0.132*	*5.177*	*98.065*	*0.723*	*0.659*	*9.845*	*0.687*
DJ- SK-13-2	*971*	*0.400*	*0.425*	*0.025*	*1.852*	*0.022*	*50.435*	*0.008*	*0.255*	*0.065*	*6.389*	*63.322*	*0.249*	*0.281*	*1.635*	*0.261*
DJ-SK-13-3	*757*	*0.575*	*0.125*	*0.012*	*1.818*	*0.006*	*47.617*	*0.003*	*0.128*	*0.040*	*1.109*	*76.249*	*0.118*	*0.076*	*10.467*	*0.047*
DJ-SK-15-1	*1540*	*0.981*	*0.425*	*0.018*	*4.128*	*0.020*	*167.973*	*0.010*	*0.239*	*0.049*	*1.984*	*98.676*	*0.518*	*0.497*	*1.287*	*0.681*
DJ-SK-16-1	*559*	*1.437*	*1.045*	*0.084*	*3.596*	*0.032*	*68.741*	*0.029*	*0.316*	*0.244*	*4.747*	*100.070*	*0.952*	*1.663*	*7.921*	*1.128*
DJ-SK-16-2	*569*	*1.815*	*1.532*	*0.139*	*5.447*	*0.033*	*130.407*	*0.043*	*0.209*	*0.277*	*4.342*	*95.419*	*1.095*	*1.826*	*10.891*	*1.224*
DJ-SK-16-3	*545*	*1.183*	*0.798*	*0.064*	*5.018*	*0.038*	*107.905*	*0.021*	*0.329*	*0.174*	*4.917*	*101.683*	*1.015*	*1.387*	*16.503*	*0.857*
DJ-SK-16-4	*430*	*1.079*	*1.199*	*0.093*	*6.735*	*0.074*	*86.049*	*0.030*	*0.512*	*0.237*	*9.498*	*123.717*	*1.018*	*2.072*	*10.704*	*1.454*
DJ-1SK-7-1	*528*	*0.400*	*0.248*	*0.036*	*1.277*	*0.052*	*25.895*	*0.005*	*3.261*	*0.046*	*9.914*	*307.657*	*0.324*	*0.321*	*1.969*	*0.607*
DJ-SK-17-2	*351*	*0.346*	*0.330*	*0.042*	*5.341*	*0.128*	*20.800*	*0.008*	*2.515*	*0.027*	*4.365*	*345.767*	*0.206*	*0.182*	*1.455*	*0.782*
BE-AN	*139*	*6.607*	*-0.002*	*0.000*	*0.081*	*-0.004*	*126.494*	*0.002*	*0.015*	*0.091*	*0.034*	*11.387*	*0.070*	*1.032*	*-0.236*	*-0.024*

Journal Pre-proof

Samples	$d^{13}C$ corr (‰)	$d^{18}O$ corr (‰)	$^{86}Sr/^{87}Sr$
DJ-SK-01-15	-0.30	-1.04	-
DJ-SK-04-15	-2.02	0.09	-
DJ-SK-05-15	0.01	-4.55	-
DJ-SK-06-15	-9.44	1.44	0.705001
DJ-SK-07-15	0.38	-0.38	0.704970
DJ-SK-08-15	1.61	0.62	0.704960
DJ-SK-09-15	1.18	-0.43	0.705075
DJ-SK-10-15	1.80	0.38	-
DJ-SK-11-15	4.35	19.61	0.705635
DJ-SK-12-15	-0.99	-1.64	-
DJ-SK-13A-15	8.92	25.34	0.705126
DJ-SK-13B-15	1.69	1.91	-
DJ-SK-14A-15	0.98	0.83	0.705375
DJ-SK-14B-15	-0.54	-0.72	-
DJ-SK-15-15	-0.27	0.41	
DJ-SK-16-15	1.55	11.40	0.705028
DJ-SK-17-15	-	-	0.705008

Tab. 3 :

Journal Pre-proof

	Aragonite	Detrital	Calcite	Mg-calcite
Sr	10500	95	1200	800
Ca	390000	2700	422000	300000
Mg	180	10000	250	50000
Sr/Ca	0.027	0.035	0.0028	0.003
Mg/Ca	0.0005	3.7	0.0006	0.17

Table 4:

Journal Pre-proof

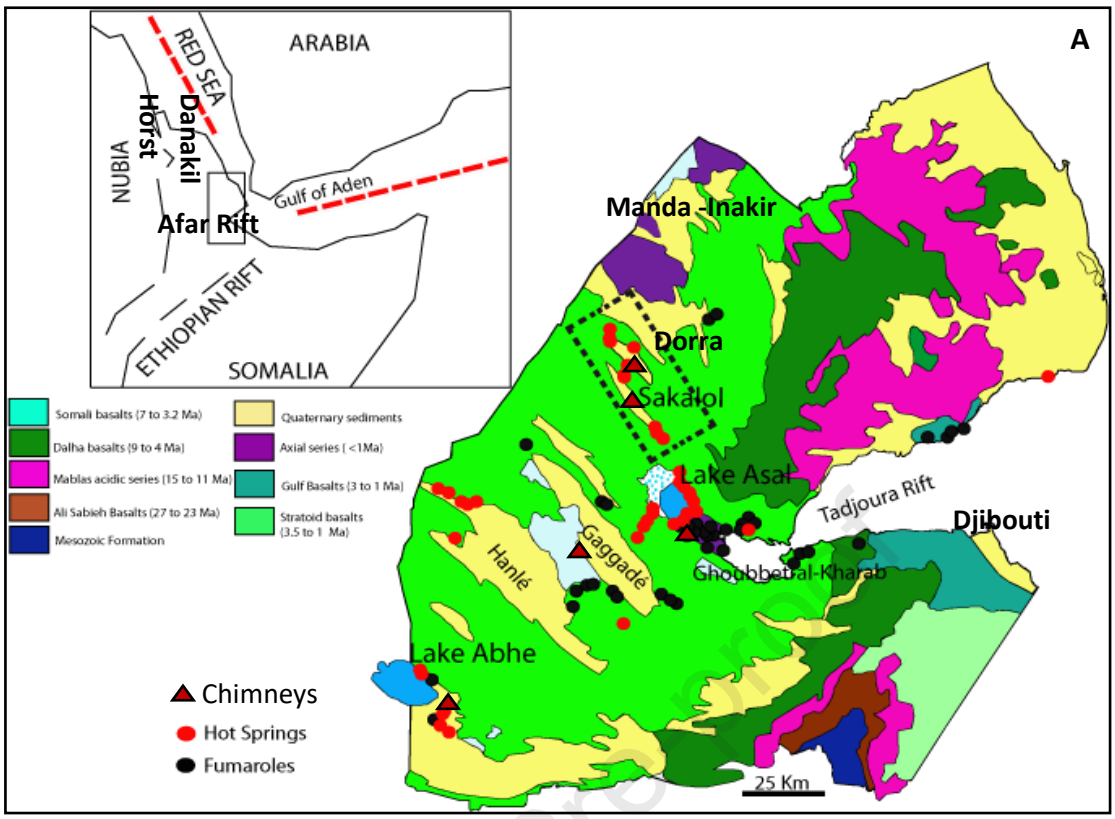
A
ARABIA
RED SEA
Danakil
Horst
NUBIA
Gulf of Aden
Afar Rift
ETHIOPIAN RIFT
SOMALIA
Somali basalts (7 to 3.2 Ma)
Dalha basalts (9 to 4 Ma)
Mablas acidic series (15 to 11 Ma)
Ali Sabieh Basalts (27 to 23 Ma)
Mesozoic Formation
Quaternary sediments
Axial series (<1Ma)
Gulf Basalts (3 to 1 Ma)
Stratoid basalts (3.5 to 1 Ma)
Manda -Inakir
Dorra
Sakalol
Lake Asal
Tadjoura Rift
Djibouti
Hanlé
Gaggade
Ghoubbet-al-Kharab
Lake Abhe
Chimneys
Hot Springs
Fumaroles
25 Km

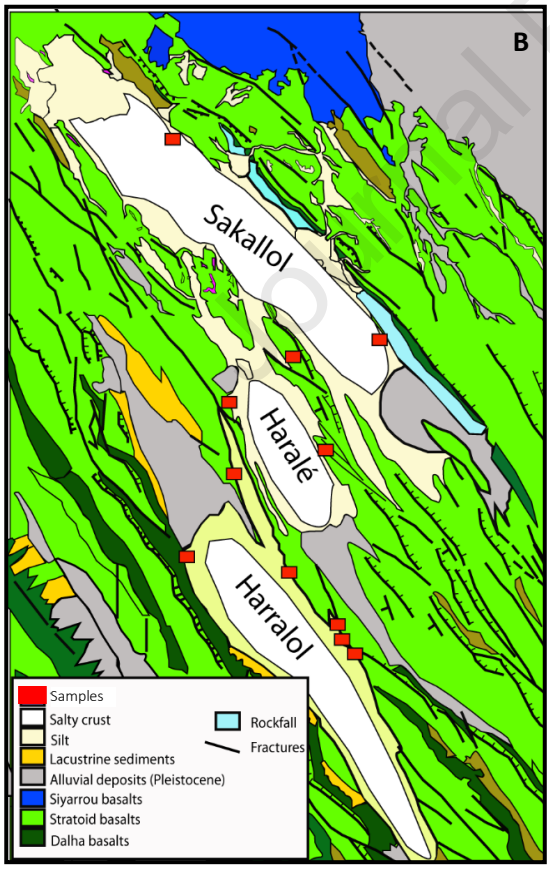
B
Sakallol
Haralé
Harralol
Samples
Salty crust
Silt
Lacustrine sediments
Alluvial deposits (Pleistocene)
Siyarrou basalts
Stratoid basalts
Dalha basalts
Rockfall
Fractures


C


D

Figure 1 :

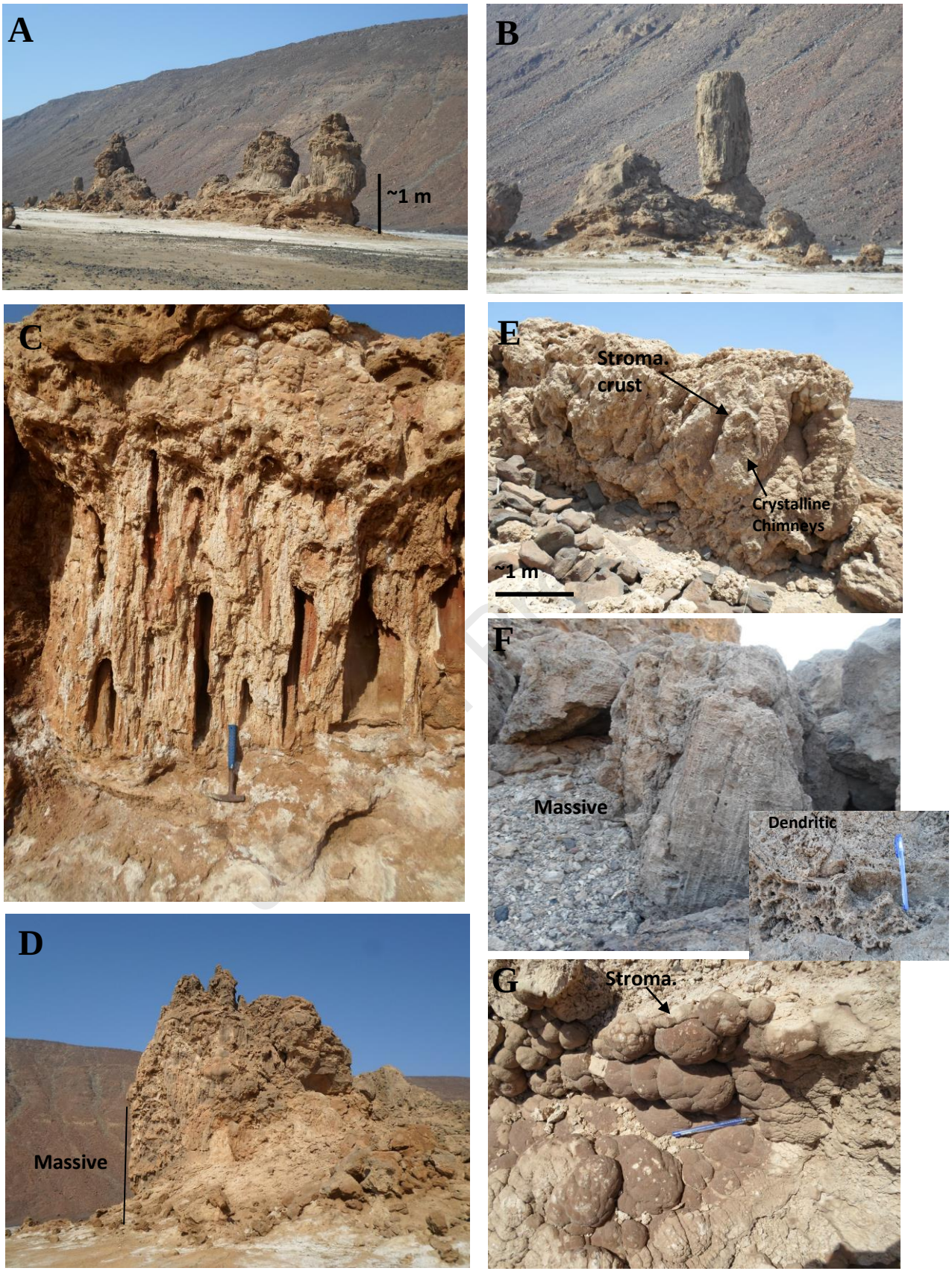
A
~1 m
B
C
E
Stroma.
crust
Crystalline
Chimneys
~1 m
F
Massive
Dendritic
D
Massive
G
Stroma.

Figure 2 :

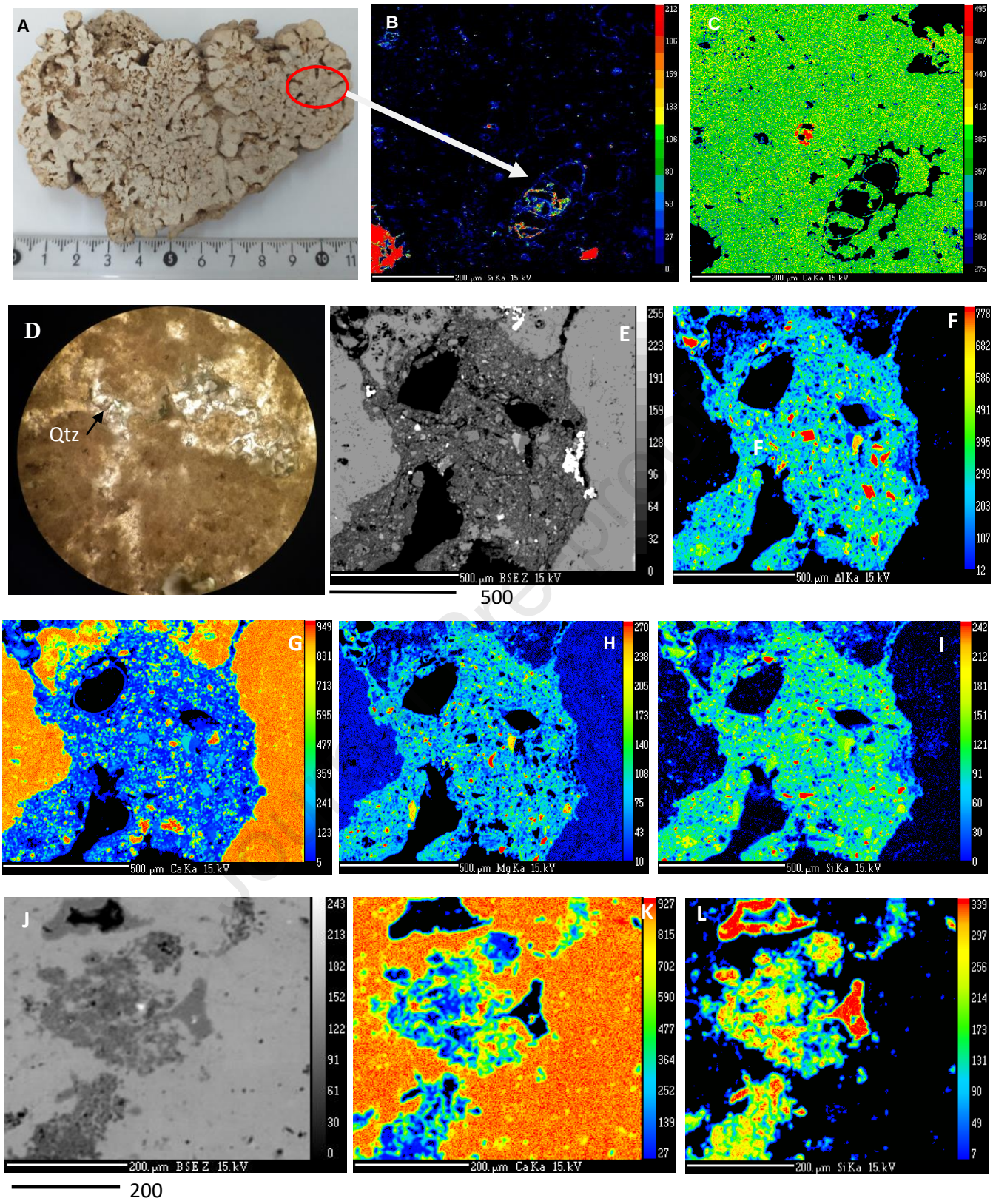

Figure 3 :

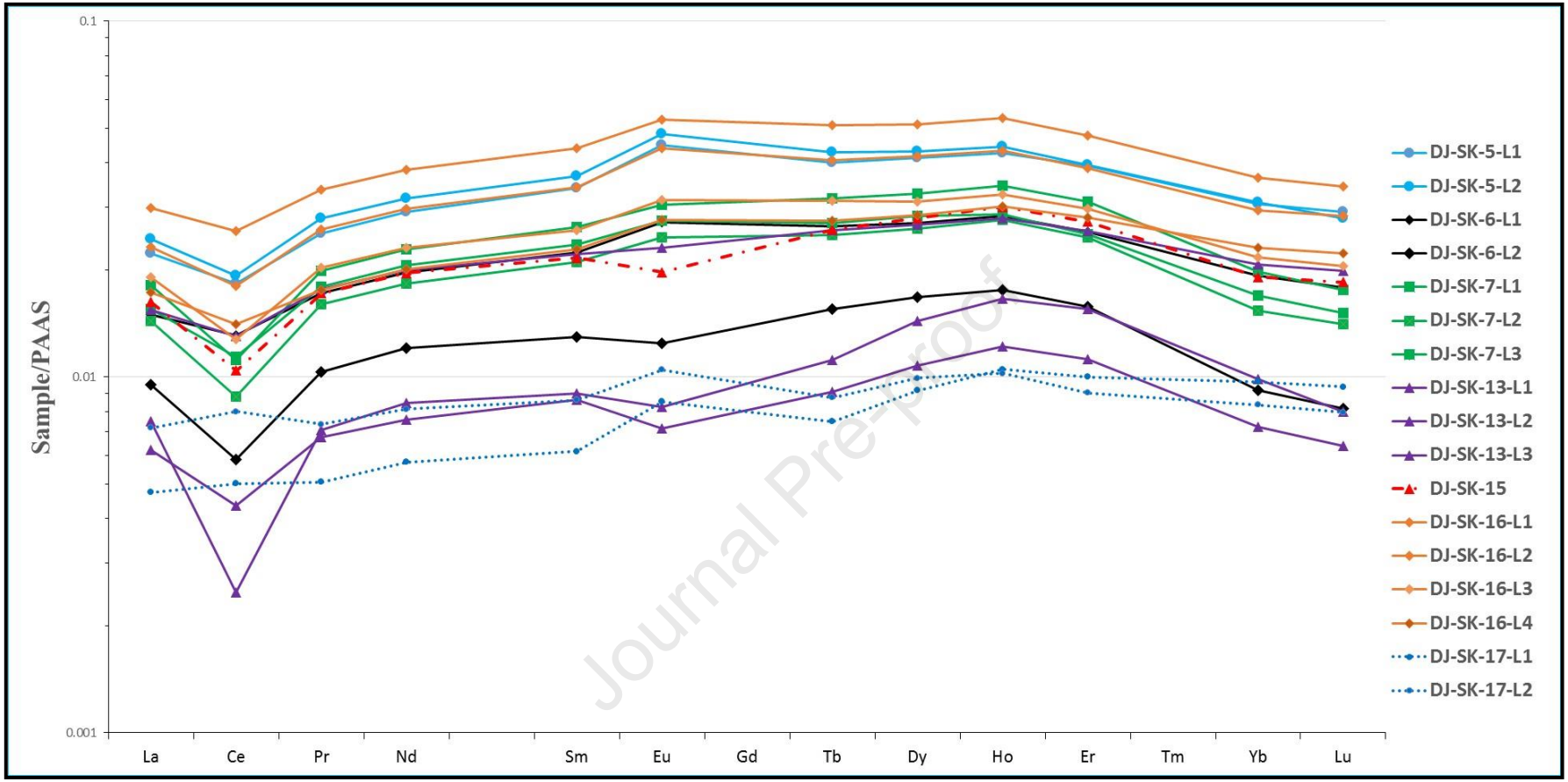
Sample/PAAS
0.1
0.01
0.001
La
Ce
Pr
Nd
Sm
Eu
Gd
Tb
Dy
Ho
Er
Tm
Yb
Lu
DJ-SK-5-L1
DJ-SK-5-L2
DJ-SK-6-L1
DJ-SK-6-L2
DJ-SK-7-L1
DJ-SK-7-L2
DJ-SK-7-L3
DJ-SK-13-L1
DJ-SK-13-L2
DJ-SK-13-L3
DJ-SK-15
DJ-SK-16-L1
DJ-SK-16-L2
DJ-SK-16-L3
DJ-SK-16-L4
DJ-SK-17-L1
DJ-SK-17-L2

Figure 4:

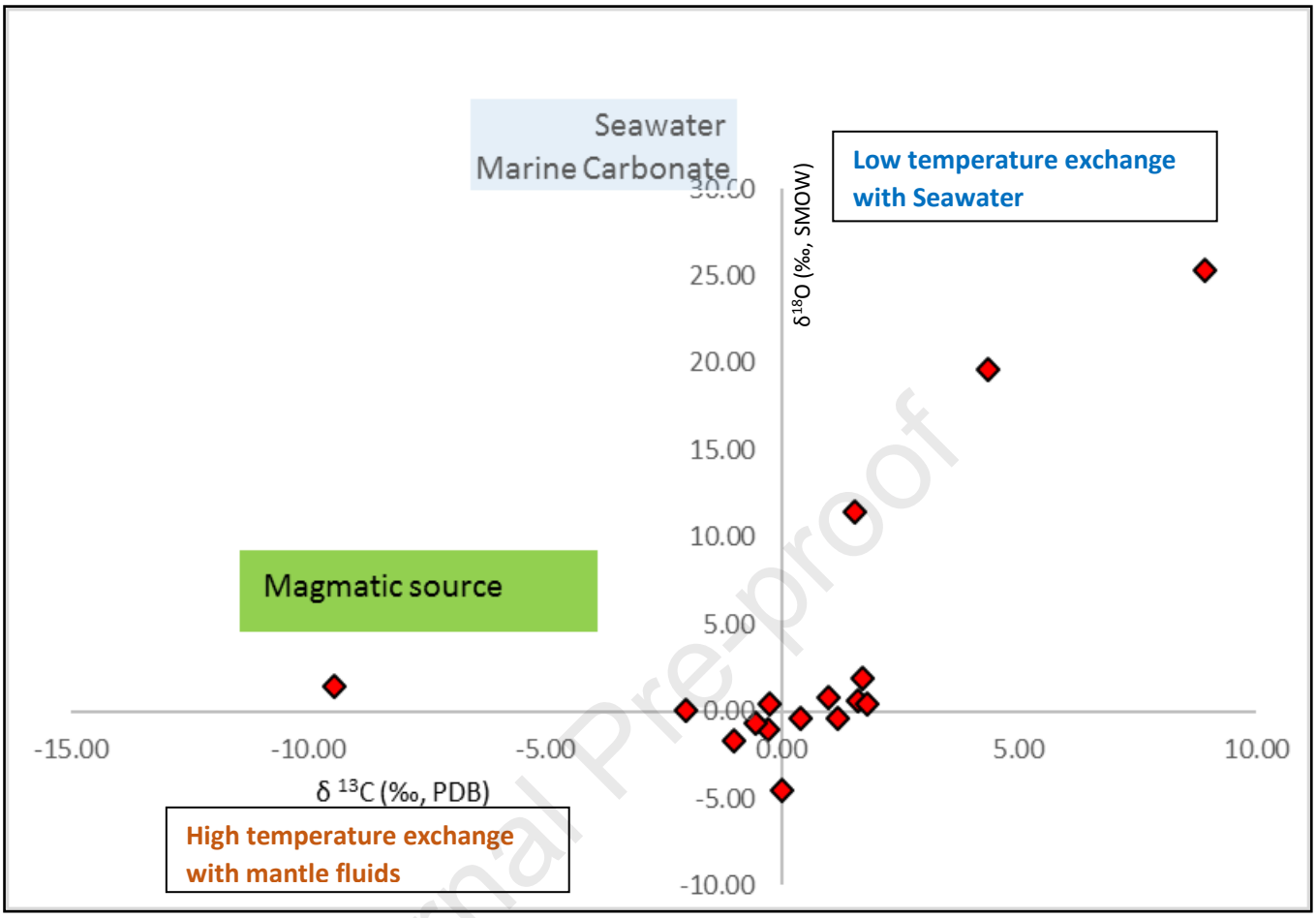

Figure 5 :

Journal Pre-proof

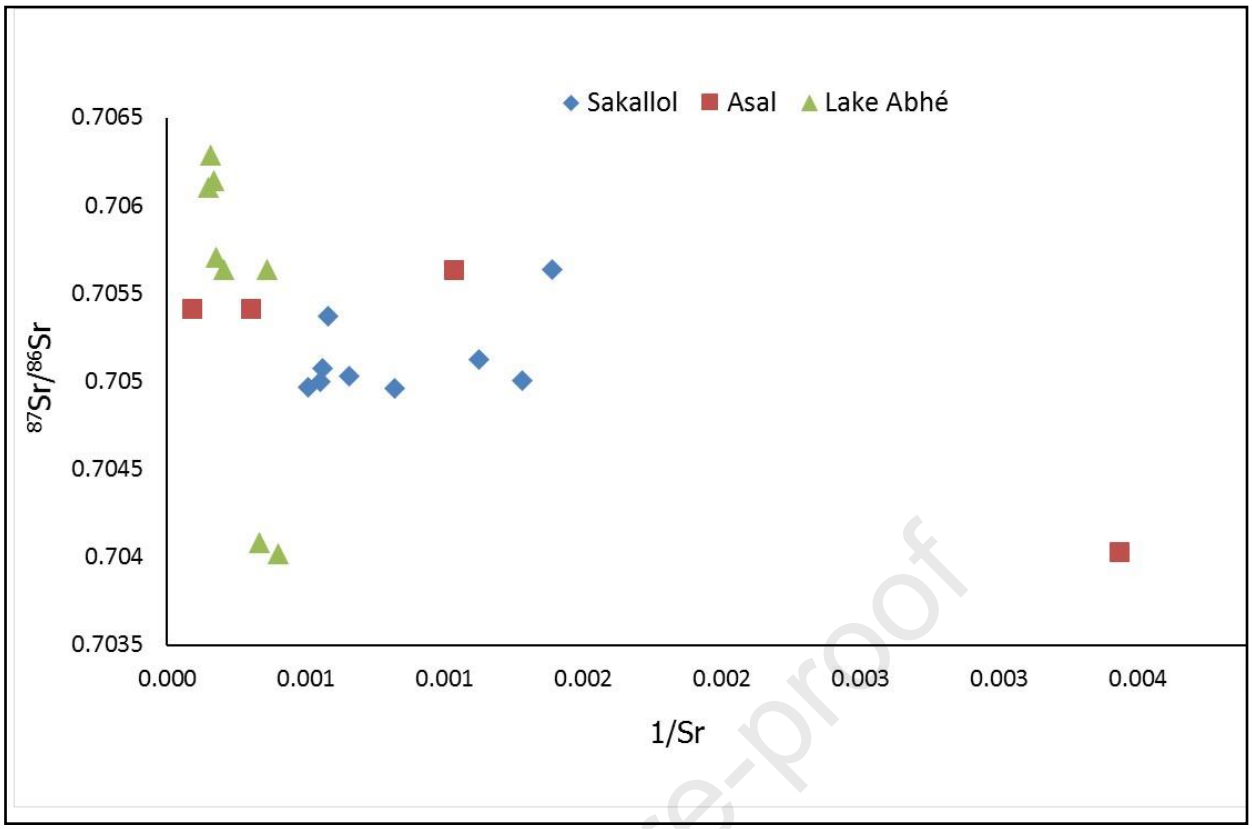

Figure 6 :

Journal Pre-proof

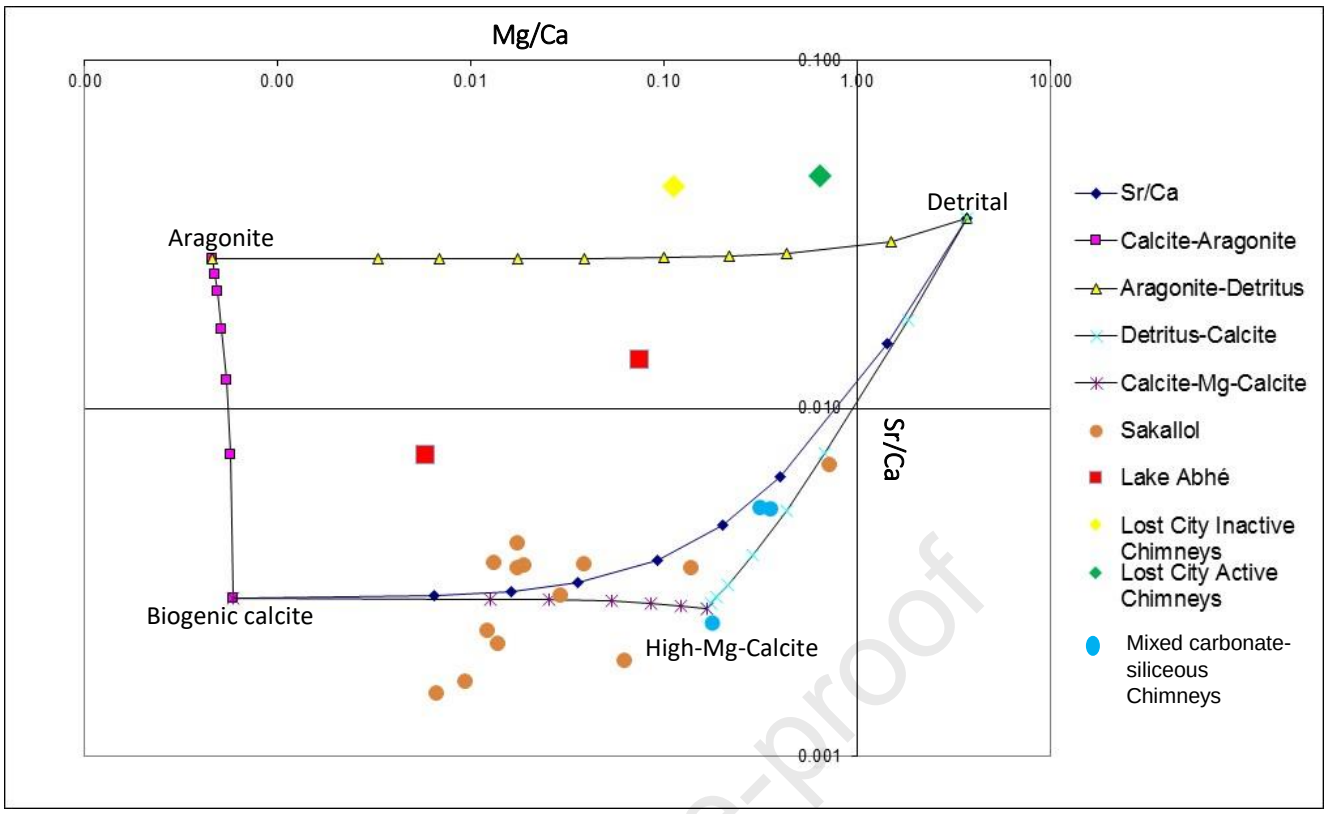

Figure 7 :

Journal Pre-proof

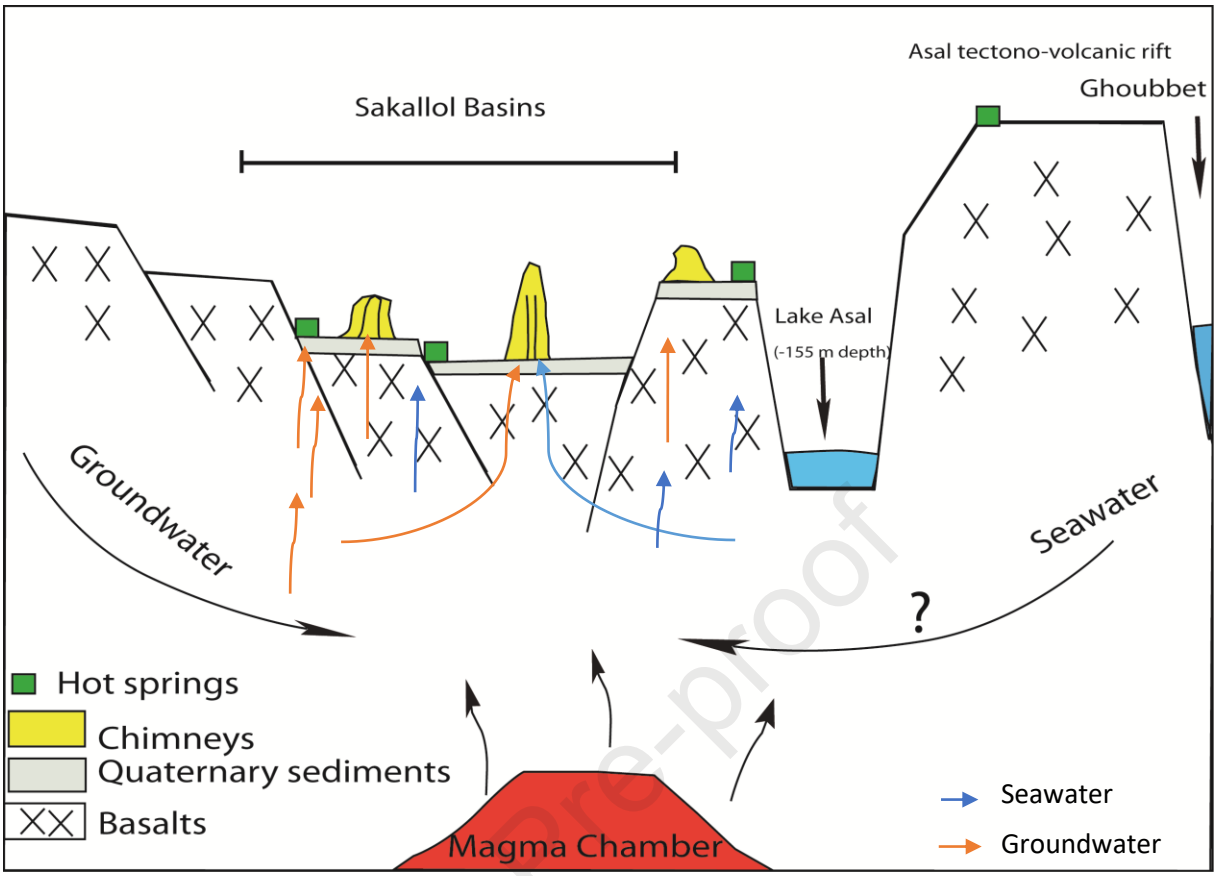

Figure 8: Schematic model of the studied area, which shows the relation between the Sakallol basins hydrothermal precipitation, groundwater and seawater from the Ghoubbet al-Kharab (Not at scale).

Journal Pre-proof

- Hydrothermal chimneys ahead of the Asal propagating rift, SE Afar Rift, Republic of Djibouti

- Radiogenic Sr isotopic compositions ($^{87}Sr/^{86}Sr$) range from 0.7049 to 0.7056
- $\delta^{18}O$ and $\delta^{13}C$ values of the chimneys range from -4.5 to 25.3‰ and from -9.44 to 8.92‰.
- Negative Ce anomaly indicate basaltic alteration
- Mixing fluids such as lake water and hydrothermal fluids which allowed the deposition of carbonate chimneys and precipitation of (and/or replacement with) silica.

Journal Pre-proof

Conflict of interest

There is no conflict of interest in this work.

Journal Pre-proof